Higher Order Mode Absorption in TTF Modules in the Frequency Range of the 3rd Dipole Band

M. Dohlus[1], V. Kaljuzhny[2], S.G.Wipf[1]

[1] Deutsches Elektronen Synchrotron, DESY, Hamburg, Germany

[2] Moscow Engineering Physics Institute, MEPI, Russia

Abstract

One of the sources of transverse emittance dilution in the superconducting e^+e^- linear collider TESLA are transverse wakefields of higher frequency modes (HOM) excited in the accelerating cavities by long trains of intense bunches. Traditionally HOM couplers (HOMC) have been designed to damp modes from the 1st and 2nd dipole bands, however measurements have shown that modes with unexpectedly high Q-factors and R/Q values occur in the 3rd dipole band. The present work quantitatively analyses the fields and their damping in the frequency range of the 3rd dipole band (~2580 MHz). In our investigation we use an S-parameter concept. For the calculations the TESLA Test Facility (TTF) accelerating module is split into several components, such as the nine-cell cavity, different types of HOM and fundamental mode couplers, cylindrical and coaxial bellows, cold windows etc., for which the S-parameters are independently calculated using the MAFIA and Microwave Studio (MWS) codes. Using the scattering matrixes of all these components, we have the ability to calculate the scattering matrix of complex sub-systems or of complete modules. The frequency dependence of the S-parameters permits us to find resonant frequencies and Q-factors of complex devices and to study the field distribution in cavities and along waveguides for a given excitation. An understanding of the damping mechanisms in the 3rd dipole band was obtained and an improved design of the HOM couplers is proposed in order to suppress those 3rd dipole band modes with high values of R/Q.

Contents

1. Introduction

One of the primary sources of transverse emittance dilution in the superconducting e^+e^- linear collider TESLA are the transverse wakefields of higher frequency modes excited in the accelerating cavities by long trains of intense bunches. These higher-order modes (HOM) must be damped to avoid multi-bunch instabilities and beam breakup. The lower the quality factors Q of the HOMs the lower the amplitude of the fields will be which are excited by the bunch train. The quality factors of the HOMs are reduced by HOM couplers (HOMC), which are mounted on the beam pipes at both ends of a TESLA 9-cell cavity [1,2,3].

Especial care was taken in designing the superconducting 9-cell cavities and the HOM couplers to achieve the desired HOM absorption of $Q \sim 10^4$ for modes with high shunt impedance in the lowest two dipole passbands. Therefore two types of HOM couplers (SACLAY type and DESY type) have been developed and tested. A cavity with one HOM coupler at each end, located in the beam pipes close to the end cells, makes up a unit. These units are always supplied with HOM couplers of the same type. For dipole modes in the third and higher passbands the beam pipes are above the cutoff frequency so that such modes can couple not only to the next absorbers but also to the absorbers of the adjacent cavity-coupler units. To damp not only monopole- and dipole- but also quadrupole-modes and modes of even higher azimuthal order the angle between two HOM couplers of one unit is chosen as 115^o. Another problem might arise from 'trapped modes', which are concentrated in the center cells and have low field amplitudes in the end cells. By an asymmetric shaping of the end cells the field of some of these modes is enhanced at one or both of the cavity ends.

Many parameters of TESLA cavity coupler units are routinely measured in a test cryostat. Although these measurements prove that the goals of the conceptual design report (CDR-goals) for higher order mode damping are fulfilled, later measurements in the TESLA Test Facility (TTF) led to a review of these requirements. To excite higher order dipole modes in the TTF, an intensity modulated beam is sent off-axis through a module with eight nine-cell cavities. A resonant mode stimulation is possible if one of the spectral lines of the beam at $n \cdot f_b \pm f_{modu}$ is close to a cavity resonance f_{cav} (with f_b the bunch repetition frequency, f_{modu} the frequency of intensity modulation and n an arbitrary integer). The modes are detected either directly by HOM coupler output signals or by beam deflections at downstream beam position monitors (BPMs). In these measurements several weakly damped dipole modes were found in higher dipole bands: one mode at the upper end of the 3rd band and further modes in the 5th and 6th dipole band. The modes in the 5th and 6th dipole band with a small shunt impedance ($<10^0$ Ω/cm^2) are quasi trapped in the nine-cell cavities. Dipole modes at the end of the 3rd passband (~2.58 GHz) with Q-value of the order of 10^6 were observed during measurements in 1998 [4] in at least three cavities of two modules (module 1 and 2) and again in later measurements (2001,[5,6]) in module 3. The weak damping of these modes was unexpected because the modes are not 'trapped' and the coupling from the end cells to the beam pipe (above cutoff) is good. The high Q mode was found only in some of the cavities and for only one of the two polarizations. The quality factor of the other polarization was approximately $2 \cdot 10^4$. As the shunt impedance ($>10^1$ Ω/cm^2) of this mode is comparable and even higher than that of the modes in the first dipole bands, special attention was paid to this problem. Several attempts were made to explain why six couplers (two HOM couplers and one

fundamental mode coupler in both adjacent beam pipes) do not provide enough damping. Explanations which were previously considered are [5, 7]:

(a) the mode is trapped due to a deformation of the cavity shape,

(b) the boundary conditions to one cavity, determined by its neighboring cavities, are such that most of the field energy of the '2.58 GHz mode' is stored inside the cavity,

(c) the couplers are inefficient for this frequency,

(d) some couplers fail because they are at a position of minimal coupling in the standing wave pattern or they are ineffective for one polarization,

(e) the field pattern is tilted so that hardly any field energy is at one side of the cavity and the couplers on the other side are at a position of minimum of coupling.

For **hypothesis (a)** we consider the simplified case of a nine-cell cavity between infinite (matched) beam pipes. For this case with a cavity with perfect geometry a quality factor of about 3000 has been calculated numerically. As the damping is proportional to the stored energy in the end cells, this energy has to be reduced by at least two orders of magnitude to explain the quality factors measured. Numerical simulations with strongly deformed cavities as well as measurements on one of the suspect cavities are in contradiction to such a strong field distortion. The numerical simulations indicate that, to account for such field distortions, geometrical errors far beyond the given tolerances and frequency shifts and much stronger than those measured, would be needed. With field measurements of a suspect and a "good" cavity between shorted beam pipes it was found that the field in the end cells is reduced by approximately 25% [5, 7]. Therefore the cavity shape distortion of the suspect cavity might explain a doubled quality factor (compared to the "good" cavity) which is still much smaller than observed.

For hypothesis (b) the field energy in an ideal cavity between shorted beam pipes with the lengths l_1 (left side) and l_2 (right side) is calculated for the highest mode of the 3rd dipole band. The damping is estimated by the following formula:

$$Q = \frac{\omega}{v_g} \frac{l_1 + l_2}{X \sum |s_\nu|^2} \quad , \tag{1}$$

with X the ratio of the time averaged energy in the beam pipes W_{pipe} to the energy in the total volume W_{tot}, $v_g \approx 0.5 c_0$ the group velocity of the H_{11} mode in the beam pipe, and s_ν the transmission coefficient of the H_{11} beam pipe wave to the load of absorber ν. This estimation is based on the following assumptions: the neighboring cavities cause a full reflection, the phase of the reflection is taken into account by a modification of the beam pipe lengths $l_{1/2} = l_{\text{pipe}} + \Delta l_{1/2}$, the modification $\Delta l_{1/2}$ is small compared to the real pipe length l_{pipe}, the power flow $P_{\text{forward}} = P_{\text{backward}}$ in the beam pipes is $W_{\text{pipe}} v_g / (2l_1 + 2l_2)$, the power transfer to the coupler loads is $P_\nu = |s_\nu|^2 (P_{\text{forward}} + P_{\text{backward}})$, the effect of the couplers is approximated by perturbation theory $Q = \omega W_{\text{tot}} / \sum P_\nu$. The assumption of a trapped mode between neighboring cavities is justified by the fact that the high Q modes are at the upper end of a passband and the affected cavities are systematically higher in frequency than their

neighbors. In Fig. 1 it can be seen that the ratio X has a broad minimum and a minimal value of approximately 0.007. The transmission coefficient s_ν to the four coupler loads is estimated with 0.2 while the transmission into the fundamental mode couplers is neglected. (The S-parameter calculations presented in this report confirm that s_ν ranges approximately between 0 and 0.4 depending on the polarization of the H_{11} wave in the beam pipe. The coupling due to the fundamental mode coupler is indeed negligible for two of the three investigated designs.) The maximal Q value of $0.7 \cdot 10^5$ which is estimated with these parameters is still one order of magnitude below the observed value.

Hypothesis (c) of inefficient couplers is tested with the same model. If we assume that the boundary conditions are so that the energy in the beam pipes is minimal (X = 0.007), the sum $\sum |s_\nu|^2$ has to be of the order of 10^{-2} to explain the high Q resonances. This is for example fulfilled if all four HOM couplers have the same 'efficiency' $|s_\nu| = 0.05$, or if three couplers are not coupling at all and the last coupler has $|s_\nu| = 0.1$. These efficiencies are much smaller than estimated and calculated.

A more precise perturbation model could help to explain the lack of coupling (**hypothesis d**):

$$P_\nu = \frac{1}{2}\left| s_{\nu,\mathrm{fh}} f_\mathrm{h} + s_{\nu,\mathrm{fv}} f_\mathrm{v} + s_{\nu,\mathrm{bh}} b_\mathrm{h} + s_{\nu,\mathrm{bv}} b_\mathrm{v} \right|^2 \qquad (2)$$

with f_h the amplitude of the horizontally polarized forward wave in the beam tube, f_v the amplitude of the vertical forward wave and b_h, b_v the amplitudes of the horizontal and vertical backward waves. The amplitudes fulfill the relation $P_{forward} = \frac{1}{2}|f_\mathrm{h}|^2 + \frac{1}{2}|f_\mathrm{v}|^2$, $P_{backward} = \frac{1}{2}|b_\mathrm{h}|^2 + \frac{1}{2}|b_\mathrm{v}|^2$. The coefficients $s_{\nu,\mathrm{fh}}$, $s_{\nu,\mathrm{fv}}$, $s_{\nu,\mathrm{bh}}$, $s_{\nu,\mathrm{bv}}$ describe the coupling of the beam tube wave to the load of coupler ν. Two effects could cause a reduced coupling: the HOM coupler is insensitive to the polarization of the high-Q mode (which is not necessarily horizontal or vertical), the coupling to forward and backward waves cancel each other. A simple estimation of the phase relations in the beam tube is not possible because this relation is sensitive to the exact resonant frequencies of the cavity and its neighbors, but this model could explain why in some of the cavities only one polarization has a high Q value.

An asymmetric field pattern as assumed in **hypothesis (e)** could be caused by the asymmetric cavity design, a deformation of the cavity shape or by different boundary conditions due to different frequency offsets of the neighboring cavities. The calculations for a cavity with perfect geometry show that the effect of the systematic asymmetry is negligible [8]. For the same reasons as discussed in (a) shape deformations can be excluded. Field asymmetries caused by boundary conditions necessarily need significant field energy at one of the boundaries. Therefore the field energy in one of the pipes has to be much higher then the minimum of the ratio $X = W_\mathrm{pipe}/ W_\mathrm{tot} = 0.007$. For such a mode with high Q the cancellation of coupling fields has to take place for only two couplers, but this cancellation has to be much better than for a more symmetric field distribution.

The present work is an attempt to quantitatively analyze the fields and their damping in the frequency range of the 3rd dipole band. In our investigation we use the S-parameter concept. The accelerating module is split into several components, which are calculated independently:

TTF nine cell cavity,

HOM coupler,

HOM coupler together with input coupler,

bellows in the beam pipe,

cold and warm windows, cold and warm bellows and doorknob of the input coupler.

These components are connected by cylindrical waveguides (beam pipe) or coaxial transmission lines (input coupler) and the remaining ports (beam pipe, coaxial port of HOM coupler, input coupler after cold window) are terminated by loads with known impedance. Using the technique described in [9], we have the ability to calculate the scattering matrix of composed complex devices and to study the frequency dependence of transmission and reflection coefficients. This permits us to find resonant frequencies and Q-factors of complex devices and to study the field distribution in cavities and along waveguides for a given excitation. By this means an understanding of the damping mechanisms in the 3rd dipole band was obtained. The essential result of our investigation is that the HOM couplers of a cavity-coupler unit are effective for only one polarization of modes in the 3rd dipole band while the other polarization is weakly damped. Additionally the standing wave pattern in the beam pipes can cause a cancellation of the coupling to some HOM dampers. A slight modification of the design of the HOM couplers is proposed to avoid the insensitivity to one polarization. The cancellation effect due to standing waves is unavoidable as the standing wave distribution depends on random frequency shifts of the cavities due to geometrical imperfections such as manufacturing tolerances. Mode computations for complete modules including cavities with a random frequency shift have been carried out to verify that the damping due to the proposed modified coupler setup is sufficient.

The S-parameter approach and S-parameter calculations for TTF module components are presented in section 2. Using the MAFIA and Microwave Studio codes, S-parameters were calculated in the 3rd dipole frequency band. It will be shown that DESY HOMCs provide a good coupling to the horizontal polarization while SACLAY HOMCs are effective for the vertical polarization.

The analysis of a cavity coupler unit between shorted beam pipes and without FMC is presented in section 3. A comparison with measurements in the CHECHIA test cryostat shows qualitative agreement. Modified HOM couplers are proposed and studied in section 3.3.

The analysis of setups with three cavity-coupler-units supplied with different types of HOM and main couplers is presented in section 4. As the DESY type and SACLAY type couplers are sensitive to different polarizations, it is not trivial to understand why high Q modes were observed in configurations with both coupler types as in module 1 and 2. For combinations of HOM and main couplers as they were used in these modules it is shown that very high quality factors can also be calculated by the numerical model if one assumes that the middle cavity is detuned by approximately 10MHz. This detuning, which is in agreement with measurements causes a weak coupling to some of the HOM couplers due to the standing wave pattern in the beam pipes. Therefore the unlucky combination of weak coupling due to polarization and standing waves still allows high Q modes even in setups with couplers to different polarizations. This behavior is not found in homogeneous groups

of cavity-coupler-units with only one type of HOM coupler and modified upstream couplers.

Modes in 8-cavity modules with DESY type couplers are analyzed in section 5. The numerical simulations allow an interpretation of the observation of localized as well as non-localized high Q modes (which couple through several cavities) in module 3 [6]. Several samples of modules with randomly detuned cavities were calculated. All modes found at the upper end of the 3rd dipole band in modules with modified upstream couplers had quality factors below 10^5.

The damping of dipole modes of the 1st and 2nd band is calculated in section 6 for cavities with modified upstream couplers.

2. S–Parameter Calculation

2.1. S–Parameter Approach and Coupled S–Parameters

One of the fruitful approaches to characterize complex multi-port devices is the scattering matrix (or S-parameter) approach. This frequency domain approach is valid for linear systems. The scattering matrix $\mathbf{S} = (s_{ik})$ relates the normalized complex amplitudes of incident and scattered waveguide waves at certain reference planes (see Fig. 2). a_k is the normalized complex amplitude of the incident wave into the k-th port, b_k is the normalized complex amplitude of the scattered wave at the same port and $P_{k\,\mathrm{inc}}$, $P_{k\,\mathrm{scat}}$ are the power fluxes of the incident and reflected waves. The amplitudes a_k, b_k as well as the coefficients s_{ik} are a function of the angular frequency $\omega = 2\pi f$, with f the frequency. Note that an independent port represents every mode in a multi modal waveguide. Therefore even a device with only one physical waveguide aperture can be considered as a multi-port device.

Let us consider a complex N-port device composed by an arbitrary number of sub-devices with known scattering matrices. Not all ports of the sub-devices correspond to external ports as there are some internal connections by waveguides with known characteristics (length, cut off frequency and attenuation) and there are some ports terminated by loads with known impedance (reflection factor).

To find the scattering matrix of this complex N-port device we use a technique described in [9,10]. Let us number the ports of the sub-devices in the following manner: 1, 2, 3, …, N are the indices of external ports, $N+1$, $N+2$, …, $N+2K-1$, $N+2K$ are the indices of connected ports (K connections) and $N+2K+1$, $N+2K+2$, …, $N+2K+M$ are the indices of ports terminated by loads (M loads with known properties). We suppose that the first connection is between the ports $N+1$ and $N+2$, the second connection is between the ports $N+3$ and $N+4$ and so on to the K-th connection between the ports $N+2K-1$ and $N+2K$. (A connection by a multi-modal waveguide corresponds to several individual port connections.) The full number of ports of the initial devices is $N+2K+M$. For the last $2K+M$ ports one can write the following relation:

$$\begin{pmatrix} a_{N+1} \\ a_{N+2} \\ \vdots \\ a_{N+2K-1} \\ a_{N+2K} \\ a_{N+2K+1} \\ a_{N+2K+2} \\ \vdots \\ a_{N+2K+M} \end{pmatrix} = \mathbf{S}_{\text{con}} \begin{pmatrix} b_{N+1} \\ b_{N+2} \\ \vdots \\ b_{N+2K-1} \\ b_{N+2K} \\ b_{N+2K+1} \\ b_{N+2K+2} \\ \vdots \\ b_{N+2K+M} \end{pmatrix}, \tag{3}$$

where $\mathbf{S}_{\text{con}}$ is the connection matrix, which has the following form:

$$\mathbf{S}_{\text{con}} = \begin{pmatrix} 0 & z_1 & & 0 & 0 & 0 & 0 & & 0 \\ z_1 & 0 & & 0 & 0 & 0 & 0 & & 0 \\ & & \ddots & & & & & & \\ 0 & 0 & & 0 & z_K & 0 & 0 & & 0 \\ 0 & 0 & & z_K & 0 & 0 & 0 & & 0 \\ 0 & 0 & & 0 & 0 & \Gamma_1 & 0 & & 0 \\ 0 & 0 & & 0 & 0 & 0 & \Gamma_2 & & 0 \\ & & & & & & & \ddots & \\ 0 & 0 & & 0 & 0 & 0 & 0 & & \Gamma_M \end{pmatrix}, \tag{4}$$

with z_k the phase factor of the k-th line and Γ_m the reflection factor of the m-th load. For loss-free, homogeneously filled waveguides the phase factor is given by:

$$z_k = \pm e^{-L_k \gamma_k} \ , \ \gamma_k = \frac{1}{c_0} \sqrt{\omega_{k\,\text{cut}}^2 - \omega^2} \ , \tag{5}$$

with L_k and $\omega_{k\,\text{cut}}$ the length and the angular cutoff frequency of the k-th line and c_0 the velocity of light. The sign in Eq. (5) has to be chosen positive if the fields of port modes on both sides of the k-th line have the same orientation, otherwise it has to be chosen negative. Fig. 3 illustrates relations (3) and (4).

For the composed (N+2K+M)-port device one can write the following relation between the complex amplitude of incident and scattered waves

$$\begin{pmatrix} \mathbf{b}_1 \\ \mathbf{b}_2 \end{pmatrix} = \begin{pmatrix} \mathbf{S}_{11} & \mathbf{S}_{12} \\ \mathbf{S}_{21} & \mathbf{S}_{22} \end{pmatrix} \begin{pmatrix} \mathbf{a}_1 \\ \mathbf{a}_2 \end{pmatrix}, \tag{6}$$

with

$$\mathbf{b}_1 = \begin{pmatrix} b_1 \\ \vdots \\ b_N \end{pmatrix},\ \mathbf{a}_1 = \begin{pmatrix} a_1 \\ \vdots \\ a_N \end{pmatrix},\ \mathbf{b}_2 = \begin{pmatrix} b_{N+1} \\ \vdots \\ b_{N+2K+M} \end{pmatrix},\ \mathbf{a}_2 = \begin{pmatrix} a_{N+1} \\ \vdots \\ a_{N+2K+M} \end{pmatrix},$$

and $\mathbf{S}_{11}$ a $N\times N$ sub-matrix, $\mathbf{S}_{12}$ a $N\times(2K+M)$ sub-matrix, $\mathbf{S}_{21}$ a $(2K+M)\times N$ sub-matrix and $\mathbf{S}_{22}$ a $(2K+M)\times(2K+M)$ sub-matrix. All these sub-matrices contain only known complex S-parameters of the sub-devices. After interconnection and loading of some ports of the initial devices one can write the following matrix equations:

$$\begin{aligned} \mathbf{b}_1 &= \mathbf{S}_{11}\mathbf{a}_1 + \mathbf{S}_{12}\mathbf{a}_2 \\ \mathbf{b}_2 &= \mathbf{S}_{21}\mathbf{a}_1 + \mathbf{S}_{22}\mathbf{a}_2 \\ \mathbf{a}_2 &= \mathbf{S}_{\text{con}}\mathbf{b}_2 \end{aligned}, \tag{7}$$

with $\mathbf{S}_{\text{con}}$ defined by relation (3). From the matrix equations (7) we can obtain the following expressions:

$$\begin{aligned} \mathbf{b}_2 &= \left[\mathbf{I} - \mathbf{S}_{22}\mathbf{S}_{\text{con}}\right]^{-1}\mathbf{S}_{21}\mathbf{a}_1 \\ \mathbf{b}_1 &= \left\{\mathbf{S}_{11} + \mathbf{S}_{12}\mathbf{S}_{\text{con}}\left[\mathbf{I} - \mathbf{S}_{22}\mathbf{S}_{\text{con}}\right]^{-1}\mathbf{S}_{21}\right\}\mathbf{a}_1 \end{aligned}, \tag{8}$$

where $\mathbf{I}$ is a unit matrix. The first expression in (8) determines the internal wave amplitudes, while the scattering matrix $\mathbf{S}$ of the external N-port system is given by the second expression

$$\mathbf{S} = \mathbf{S}_{11} + \mathbf{S}_{12}\mathbf{S}_{\text{con}}\left[\mathbf{I} - \mathbf{S}_{22}\mathbf{S}_{\text{con}}\right]^{-1}\mathbf{S}_{21}\ . \tag{9}$$

The transverse electromagnetic field due to the waveguide mode which is considered for the k-th line (between the ports $N + 2k - 1$ and $N + 2k$) is described by the following equations

$$\begin{aligned} \mathbf{E}_{\text{t},k}(\mathbf{r}_t, z) &= \mathbf{E}_{tn,k}(\mathbf{r}_\text{t})\, Z_k^{1/2}\left(b_{N+2k-1}e^{-\gamma_k z} + a_{N+2k-1}e^{\gamma_k z}\right) \\ \mathbf{H}_{\text{t},k}(\mathbf{r}_\text{t}, z) &= \mathbf{e}_z \times \mathbf{E}_{tn,k}(\mathbf{r}_\text{t})\, Z_k^{-1/2}\left(b_{N+2k-1}e^{-\gamma_k z} - a_{N+2k-1}e^{\gamma_k z}\right) \end{aligned}, \tag{10}$$

with $\mathbf{E}_{\text{t},k}$ the transverse electric field, $\mathbf{H}_{\text{t},k}$ the transverse magnetic field, $\mathbf{r}_\text{t}$ the transverse position in the waveguide, z the longitudinal position in the waveguide with respect to the reference plane of port $N + 2k - 1$, $\mathbf{E}_{tn,k}$ the normalized transverse electric field in the waveguide, Z_k the wave impedance and γ_k the propagation constant as defined in Eq. (5). The normalization condition for $\mathbf{E}_{tn,k}$ is

$$\int_{\substack{\text{waveguide} \\ \text{crossection}}} \mathbf{E}_{tn,k}(\mathbf{r}_\text{t}) \cdot \mathbf{E}_{tn,k}(\mathbf{r}_\text{t})\, dA = 1\ .$$

The wave impedance is related to the propagation constant by $Z_k = Z_0 \cdot \gamma_k c_0 / j\omega$ for TM modes and by $Z_k = Z_0 \cdot j\omega / \gamma_k c_0$ for TE modes, with Z_0 the free space impedance.

With the above technique we have the ability to calculate the scattering matrix of complex devices composed of several sub-devices and to study the dependence of S-parameters as a function of frequency. The frequency dependence permits us to find resonant frequencies and to estimate Q factors. For these resonances the field distributions along the connecting waveguides and in the cavities can be calculated.

The method for calculating the cavity fields for given wave amplitudes at the boundaries will be described in section 2.2.1.

2.2. Cavity

The accelerating cavity together with welded HOM couplers is shown in Figs. 4, 5 [3]. It is a standing wave nine cell structure made of niobium. The fundamental mode is a π mode (the direction of the electric field alternates from cell to cell) and has a frequency of 1.3 GHz. The shape of the cells was optimized in order to avoid high local fields and multipacting. The end half-cells have a slightly different shape in order to ensure the field flatness in all cells. The power coupler is placed downstream. In the following section the term "cavity" is used only for the rotationally symmetric nine-cell structure together with beam pipes of a certain length (l_{upstream}, $l_{\mathrm{downstream}}$). The lengths of the beam pipes are chosen for numerical reasons: the pipes have to be long enough so that all waveguide modes besides the H_{11} mode are sufficiently damped.

2.2.1. Numerical Calculation

The S-parameters for a TESLA cavity with design geometry [2] are calculated by an eigenmode technique as described in [11]. Therefore the first 60 dipole modes of a cavity between beam pipes are calculated by the MAFIA eigenmode solver [12] for magnetic boundary conditions. The discretization with 107000 mesh cells is described in [13]. The impedance matrix **Z** is approximated by:

$$\mathbf{Z}_{\mathrm{A}}(\omega) = \sum_{\nu} \frac{j\omega}{\omega_\nu^2 - \omega^2} \mathbf{A}_\nu \quad , \tag{11}$$

with

$$\mathbf{A}_\nu = \frac{1}{2}\begin{pmatrix} u_{\nu,1} \\ u_{\nu,2} \end{pmatrix}\begin{pmatrix} u_{\nu,1} & u_{\nu,2} \end{pmatrix}$$

$$u_{\nu,1/2} = \int\limits_{\substack{\text{up-/downstream} \\ \text{boundary plane}}} \frac{\mathbf{E}_\nu}{\sqrt{W_\nu}} \cdot \mathbf{E}_{tn,\mathrm{H11}}\, dA \quad ,$$

and ν the mode number, $\mathbf{E}_\nu$ the electrical field of mode ν, W_ν the total electromagnetic field energy of mode ν and $\mathbf{E}_{tn,\mathrm{H11}}$ the normalized transverse electric field of the H_{11} mode in the beam pipe as defined before. This approximation can be improved by a correction term $\mathbf{Z}_{\mathrm{C}}(\omega)$ that can be calculated from the eigensolutions for electric/electric, electric/magnetic and magnetic/electric boundary conditions at the ends of the beam pipes [11]. The coefficients of the correction term are purely imaginary, and these imaginary parts have a smooth monotone frequency dependence in the frequency range that is covered by the mode expansion. Therefore the correction function can be interpolated from a coarse mesh to any frequency point. The scattering matrix, which is calculated by

$$\begin{aligned} &\mathbf{S}(\omega) = \left(\mathbf{Z}(\omega) + Z_{\mathrm{H11}}(\omega)\mathbf{I}\right)^{-1}\left(\mathbf{Z}(\omega) - Z_{\mathrm{H11}}(\omega)\mathbf{I}\right) \\ &\text{with} \quad \mathbf{Z}(\omega) = \mathbf{Z}_A(\omega) + \mathbf{Z}_{\mathrm{C}}(\omega) \end{aligned} \quad , \tag{12}$$

fulfils the unitary condition exactly. The scattering parameters of the TESLA cavity can be seen in Figs. 6, 7, 8 and 9. Due to the asymmetry of the end cells the phases of the reflection coefficients s_{11} and s_{22} are not identical (compare Fig. 8). The resonance peak of the transmission coefficient s_{12} with the highest frequency in Fig. 7 is at 2.57715 GHz and has a 3 dB bandwidth of 0.904 MHz. Therefore the last mode of the 3rd dipole band has a quality factor of about 2850 for a cavity between matched beam pipes.

The eigenmode technique used has several advantages. The first is that the numerical effort is nearly independent of the bandwidth of any resonance and the calculation is valid for a very wide frequency range. For the TESLA cavity the entire range from DC to 3.5GHz is covered. In contrast to this an analysis by direct frequency domain calculations requires many independent computations on a fine frequency mesh. For time domain calculations, pulse responses have to be calculated until a significant part of the field energy, which was delivered by the excitation, has propagated through the waveguide ports of the system. In Figs. 10, 11, 12 and 13 the results of a time domain calculation (Fourier transformation of the transients in 0.38 μsec, $2.7 \cdot 10^6$ time steps, [14]) are compared with the modal analysis. The error of the time domain calculation due to the incomplete transients can be seen clearly in these figures. Especially at the upper end of the passband this error and the violation of the energy conservation ($|s_{11}|^2 + |s_{21}|^2 = 1$) are far too large for a calculation of high Q modes.

As the resonant fields in a cavity in a complicated environment are at least similar to those in a cavity between closed beam tubes, the calculation of eigenmodes gives useful information about field types and distributions. Fig. 14 shows the electric field distribution of the highest mode of the 3rd dipole band with the frequency 2.57682 GHz (for arbitrary boundary conditions as described in the caption). The r component and the derivative $\partial / \partial r$ of the z component of this field on the axis of the cavity are shown in Fig. 15. The phase advance of this field is approximately 2π per cell, and the beam has the same phase advance for 2×1.3 GHz (twice the fundamental mode frequency). Therefore the beam is nearly synchronous to the mode so that a strong interaction is possible. The excitation of the field energy of the ν-th dipole mode is proportional to $r_d^2 k_{\parallel,\nu}$ and the transverse kick observed by a test particle is proportional to $r_t k_{\perp,\nu}$, with $k_{\parallel,\nu}$ the loss parameter, $k_{\perp,\nu}$ the kick parameter

$$k_{\parallel,\nu} = \frac{|V_\nu|^2}{4W_\nu}$$

$$k_{\perp,\nu} = \frac{c_0}{\omega_\nu} k_{\parallel,\nu} \quad , \tag{13}$$

$$V_\nu = \int \frac{\partial E_{z,\nu}}{\partial r} \exp\left(j \frac{\omega_\nu}{c_0} z \right) dz$$

with r_d the radial offset of the drive beam and r_t the radial offset of the test particle. (For more details see [15,8].) The loss parameters of all modes used for the S parameter calculation can be seen in Fig. 16. The strongest loss parameter of about $8 \cdot 10^{14}$ V/(Cm^2) is found for the last mode of the 3rd dipole band. As the boundary condition significantly influences this parameter, the field energy in the beam pipes is

not negligible and a sufficient damping by absorbers in the beam pipe should be possible. For a detailed analysis of monopole, dipole and quadrupole eigenmodes in a wide frequency range see [8].

Another advantage of the eigenmode approach is that the electromagnetic fields in the cavity can be approximated by a truncated mode expansion for any frequency and any excitation by wave amplitudes a_1, a_2:

$$\begin{aligned}\mathbf{E}(\mathbf{r}) &\approx \sum_\nu \alpha_\nu \frac{\mathbf{E}_\nu(\mathbf{r})}{\sqrt{W_\nu}} \\ \mathbf{H}(\mathbf{r}) &\approx \frac{j}{\mu_0}\sum_\nu \frac{\alpha_\nu}{\omega_\nu}\frac{\mathrm{curl}\{\mathbf{E}_\nu(\mathbf{r})\}}{\sqrt{W_\nu}}\end{aligned}, \tag{14}$$

with

$$\alpha_\nu = \frac{1}{2}\frac{1}{\sqrt{Z_{\mathrm{H11}}}}\frac{j\omega}{\omega_\nu^2-\omega^2}\begin{pmatrix}u_{\nu,1} & u_{\nu,2}\end{pmatrix}(\mathbf{I}-\mathbf{S})\begin{pmatrix}a_1\\ a_2\end{pmatrix}. \tag{15}$$

This is demonstrated for an eigenmode calculation of a cavity between electrical boundaries. Therefore the eigenmode problem $\mathbf{S}(\omega)\mathbf{a} = -\mathbf{a}$ is solved (with S given by Eq. (12)) and the fields are calculated by Eqs. (14, 15). This expansion uses only fields $\mathbf{E}_\nu(\mathbf{r})$ which have been calculated for magnetic boundary conditions. In Fig. 17 and 18 the electrical field computed by this method is compared with the direct solution of the eigenmode problem for electric boundary conditions.

2.2.2. Two Polarizations

The 2×2 scattering matrix which is calculated by Eq. (12) corresponds to one polarization of the dipole fields in the cavity. The matrix for both polarizations follows as

$$\mathbf{S}_{2\mathrm{pol}} = \begin{bmatrix} s_{11,1\mathrm{pol}} & 0 & s_{12,1\mathrm{pol}} & 0 \\ 0 & s_{11,1\mathrm{pol}} & 0 & s_{12,1\mathrm{pol}} \\ s_{21,1\mathrm{pol}} & 0 & s_{22,1\mathrm{pol}} & 0 \\ 0 & s_{21,1\mathrm{pol}} & 0 & s_{22,1\mathrm{pol}} \end{bmatrix}, \tag{16}$$

with $s_{\mu\nu,1\mathrm{pol}}$ the coefficients of the S matrix for one polarization. The four ports are named 1h, 1v, 2h and 2v. The number stands for the side of the cavity (1 for upstream, 2 for downstream) and the letter for the polarization (h for horizontal, v for vertical). The horizontal polarization is related to the *x* component of the electrical field on the axis of the beam pipe, the vertical polarization is related to the *y* component (cf. coordinate system in Fig. 5). In this report, the normalized transverse fields $\mathbf{E}_{\mathrm{t1h,H11}}$,$\mathbf{E}_{\mathrm{t2h,H11}}$ of ports with horizontal polarization are chosen so that their *x* component is positive, the normalized transverse fields $\mathbf{E}_{\mathrm{t1v,H11}}$,$\mathbf{E}_{\mathrm{t2v,H11}}$ of vertical ports have a positive *y* component. For a cavity with perfect symmetry of revolution there is no coupling between the two polarization planes.

A simple model is used to study the effect of detuning and polarization. We assume that all cells of the cavity have a slight elliptical shape with respect to the main axes

$$\begin{aligned} p &= x\cos\varphi + y\sin\varphi \\ q &= -x\sin\varphi + y\cos\varphi \end{aligned} \quad . \tag{17}$$

Therefore the S matrix has the form

$$\mathbf{S}'_{2\mathrm{pol}} = \mathbf{R}(-\varphi)\begin{bmatrix} s_{11,p} & 0 & s_{12,p} & 0 \\ 0 & s_{11,q} & 0 & s_{12,q} \\ s_{21,p} & 0 & s_{22,p} & 0 \\ 0 & s_{21,q} & 0 & s_{22,q} \end{bmatrix}\mathbf{R}(\varphi) \tag{18}$$

with

$$\mathbf{R}(\varphi) = \begin{bmatrix} \cos\varphi & \sin\varphi & 0 & 0 \\ -\sin\varphi & \cos\varphi & 0 & 0 \\ 0 & 0 & \cos\varphi & \sin\varphi \\ 0 & 0 & -\sin\varphi & \cos\varphi \end{bmatrix} . \tag{19}$$

Further we assume that the coefficients $s_{\mu\nu,p}$ and $s_{\mu\nu,q}$ are identical to the coefficients $s_{\mu\nu,1\mathrm{pol}}$ of the ideal cavity, with exception of frequency shifts $\delta f_p = \delta\omega_p/2\pi$, $\delta f_q = \delta\omega_q/2\pi$:

$$\begin{aligned} s_{\mu\nu,p}(\omega) &= s_{\mu\nu,1\mathrm{pol}}(\omega - \delta\omega_p) \\ s_{\mu\nu,q}(\omega) &= s_{\mu\nu,1\mathrm{pol}}(\omega - \delta\omega_q) \end{aligned} \quad . \tag{20}$$

The transformation of the S matrix is described by only three deformation parameters:

$$\mathbf{S}'_{2\mathrm{pol}} = \mathbf{T}\left[\mathbf{S}_{2\mathrm{pol}}, \varphi, \delta\omega_p, \delta\omega_q\right] . \tag{21}$$

A more flexible deformation model could be used, if it were possible to describe the scattering matrix of the nine-cell cavity by the series connection

$$\mathbf{S}_{2\mathrm{pol}} = \mathbf{S}_1 \otimes \mathbf{S}_2 \otimes \ldots \otimes \mathbf{S}_9 \tag{22}$$

of the nine scattering matrices $\mathbf{S}_1$, … , $\mathbf{S}_9$ of the individual cells, and to apply individual transformations to all cells:

$$\mathbf{S}'_{2\mathrm{pol}} = \mathbf{T}\left[\mathbf{S}_1, \varphi_1, \delta\omega_{p,1}, \delta\omega_{q,1}\right] \otimes \mathbf{T}\left[\mathbf{S}_2, \varphi_2, \delta\omega_{p,2}, \delta\omega_{q,2}\right] \otimes \ldots \otimes \mathbf{T}\left[\mathbf{S}_9, \varphi_9, \delta\omega_{p,9}, \delta\omega_{q,9}\right] \quad . \tag{23}$$

2.3. Couplers

2.3.1. Orientation of the Upstream HOM Coupler

The orientation of the upstream higher order mode coupler (denoted as K2 coupler) can be seen in Fig. 5 and 19. The cavity-coupler unit is equipped either with DESY-type (welded) or SACLAY-type (demountable, with flange) HOM couplers. For both types the coupling to the RF fields is made through a loop. The loop couples capacitively to a 50 Ohm transmission line, which is terminated outside the cryostat by a load. The diameter of the beam pipe d_{pipe} is 78 mm, the diameter of the coupler cylinder d_{coupler} is 40 mm, the angle between the horizontal axis and the axis of the

coupler cylinder is -150^{o}. The two coupler types differ by the orientation of the loop and the realization of the notch filter that prevents the damping of the accelerating mode.

The time domain solver of MWS [16] is used to calculate the S parameters of both coupler types in the frequency range from 2.4 to 2.65 GHz. Therefore they are discretized on a rectangular mesh with the main axes as shown in Fig. 20. The axis of the coupler cylinder is identical to the *u*-axis, the beam pipe ranges from $w = -80$ mm to 80 mm. The device is computed as a five port system: port 1 is the coaxial port, ports 2h and 2v are waveguide ports with the reference plane at $w = -45$ mm and the ports 3h and 3v have their reference plane at $w = 45$ mm. The normalized transverse fields $\mathbf{E}_{t2h,H11} = \mathbf{E}_{t3h,H11}$ and $\mathbf{E}_{t2v,H11} = \mathbf{E}_{t3v,H11}$ of the waveguide ports are chosen as shown in Fig. 21. Therefore the ports 2h and 3h are related to the horizontal polarization while 2v and 3v are related to the vertical polarization.

A slight modification of the geometry of the DESY coupler can be seen in Fig. 22. This modification was necessary to avoid an unfavorable discretization of the coaxial transmission line.

2.3.2. Orientation of the Downstream HOM Coupler and the Main Coupler

The downstream higher order mode coupler (denoted as K1 coupler) and the main coupler (power coupler) have the same longitudinal position and are computed together. The shape of the HOM coupler is the same as on the upstream side of the cavity, but the orientation is different (cf. Fig. 5 and 23). The geometrical transformation from coupler K2 to coupler K1 is a rotation of 5^{o} around the *z*-axis and a 180^{o} rotation around the *y*-axis. (This is not the same as a rotation of 115^{o} around the *z*-axis although the angle between the two HOM coupler axes is 115^{o} as mentioned in the introduction.)

The three types of main couplers, which are used in TTF, are shown in Fig. 25. For all types the outer diameter of the coaxial transmission line is 40 mm, but for the DESY-I and FNAL types the inner diameter is chosen for an impedance of 50 Ohm while the DESY-II type has an impedance of 70 Ohm. Besides this, the shape of the antenna tips, the location and size of the bellows, the cold windows and the connection to the warm waveguides are different. As most of these differences are beyond the reference plane of the main coupler port, only the different tip shapes and different diameters of the inner conductor have to be taken into account for the S parameter calculation. The other differences are the subject of separate calculations. The penetration depth of the coupler tip is used to adjust the external quality of the accelerating mode (typically $2 \cdot 10^{6}$ in TTF). In [17] an external quality of $2 \cdot 10^{6}$ has been calculated for the DESY-II coupler with a penetration depth of 9 mm. The same penetration depth is used for the discretization of the other coupler types.

The frequency range, the beam pipe lengths and the positions of the reference planes are chosen as for the S parameter calculation of the upstream HOM coupler. The axes of the rectangular mesh, which is used for the discretization, can be seen in Fig. 24. The HOM/main coupler system is computed as a six port system: port 1 is the coaxial port of the HOM coupler, ports 2h and 2v are the upstream waveguide ports ($w = -45$ mm), ports 3h and 3v are the downstream waveguide ports ($w = 45$ mm) and port 4 is the main coupler port. The normalized transverse fields of the waveguide ports are chosen so that the 2h/3h ports are related to the horizontal and the 2v/3v ports to the vertical polarization (cf. Fig. 26).

MWS [16] is only able to calculate ports parallel to the surface of the rectangular mesh. Therefore it was necessary to bend the coaxial transmission line of the main coupler as shown in Fig. 24.

2.3.3. Spatial Resolution

The S parameters of both types of HOM couplers (upstream) and of several combinations of HOM and main couplers (downstream) have been calculated as shown in the following table. To probe the sensitivity of the numerical results on the spatial resolution, most setups have been computed for two mesh line densities (MWS parameter: 30 lines/wavelength and 50 lines/wavelength). The number of mesh points for the higher and lower resolution are listed in the table, with those for the lower resolution in brackets. For one example, the DESY/DESY-II downstream coupler pair, this sensitivity can be seen in Fig. 27.

HOM coupler	Main Coupler	u_{min}, u_{max} (mm)	v_{min}, v_{max} (mm)	w_{min}, w_{max} (mm)	mesh points (10^3)
DESY		-39/109.2	-39/39	-80/80	578 (186)
DESY	DESY-II	-79.9/109.2	-57.5/39	-80/80	1181 (371)
DESY	DESY-I	-88.9/109.2	-63.8/39	-80/80	2306 (719)
DESY	FNAL	-79.9/109.2	-57.5/39	-80/80	1203 (362)
DESY	no inner conductor	-83.5/109.2	-66.9/39	-80/80	995 (298)
SACLAY		-39/122.5	-39/39	-80/80	919 (270)
SACLAY	DESY-II	-80/122.5	-57.5/39	-80/80	1651 (513)
SACLAY	DESY-I	-88.9/122.5	-63.8/39	-80/80	3056 (916)
SACLAY	FNAL	-80/122.5	-57.5/39	-80/80	1653 (489)
SACLAY	no inner conductor	-83.5/122.5	-66.9/39	-80/80	1394 (414)

2.3.4. DESY HOM Couplers

The coupling from the beam pipe ports to the coaxial HOM coupler port can be seen in Fig. 28 for the upstream DESY HOM coupler, and in Fig. 29 for the downstream DESY/DESY-II HOM/main coupler pair. The corresponding diagram for the DESY/DESY-I HOM/main coupler pair looks very similar and is therefore not shown here. It is remarkable that both HOM couplers provide a very good coupling to the horizontal polarization (0.35 … 0.4) while the coupling to the vertical polarization is one order of magnitude weaker although the orientation of the couplers is very different (cf. Fig. 19, 23).

The similarity of Fig. 28 and 29 is essentially caused by the geometry transformation from coupler K2 to coupler K1: rotation of 5^o around the *z*-axis, 180^o rotation around the *y*-axis. If one neglects the 5^o rotation around the *z*-axis, the horizontal and vertical planes are transformed into themselves. Therefore the following pairs of scattering parameters should be comparable:

Upstream	downstream

$s_{1,2h}$	$-s_{1,3h}$
$s_{1,3h}$	$-s_{1,2h}$
$s_{1,2v}$	$s_{1,3v}$
$s_{1,3v}$	$s_{1,2v}$

The different sign of the horizontal parameters is caused by a change of the orientation of the port modes. The other differences between these pairs come from the 5^o rotation around the *z*-axis and the presence of the main coupler.

The weak coupling to the horizontal polarization is not a principle property of the loop coupling but a feature of the DESY HOM coupler. In the following it will be shown that the SACLAY HOM coupler behaves quite differently, and that the coupling of a loop to a certain polarization is determined by boundary conditions inside of the HOM coupler.

As both DESY HOM couplers and the main coupler are much more effective for the horizontal polarization than for the vertical, one can expect that the *Q* values of modes with vertical polarization are significantly higher than that of horizontal polarized modes.

2.3.5. SACLAY HOM Couplers

The transmission parameters from the beam pipe ports to the port of the SACLAY HOM coupler can be seen in Fig. 30 for the upstream side. Fig. 31 shows the same parameters for the downstream coupler in combination with a DESY-II main coupler. (The combination SACLAY/FNAL HOM/main coupler behaves very similarly.) The upstream SACLAY coupler provides a very good coupling to the vertical but a much weaker coupling to the horizontal polarization. This is the reverse of the behavior of the DESY HOM coupler. For the same reasons as discussed before, the downstream coupler shows the same sensitivity and insensitivity as the upstream coupler.

In cavities with SACLAY HOM couplers a good damping of modes with vertical polarization can be expected. The damping of modes with horizontal polarization depends additionally on the power absorption through the main coupler. Therefore the reflection coefficient of the window (cf. Fig. 25) has to be taken into account.

The experimental setup in Fig. 32 was used to measure qualitatively the transmission from a beam pipe wave with adjustable polarization to the port of the HOM coupler. Therefore the coupler is attached to a beam pipe which is open on both sides. The open pipes are used instead of waveguide loads, which were not available. (The reflection coefficient from the pipe ends is below 0.2.) Four antennas in a plane close to the front end of the beam pipe penetrate radially into the beam pipe. The antenna axes build an orthogonal cross. Only one of the antennas is stimulated, while loads terminate the others. The orientation of the adjustable angle φ, between the axes of the stimulating antenna (port 1) and the HOM coupler (port 2), can be seen in the figure. The transmission between these ports is measured with a network analyzer and can be seen in Fig. 33 for three frequencies (2.57, 2.58 and 2.60 GHz). The measurement setup (a) corresponds to a stimulation of the HOM coupler from the cavity side, setup (b) corresponds to a stimulation from the other side. The horizontal plane of the upstream coupler agrees with the angular position of 30^o in Fig. 33a and with the angle -30^o in Fig. 33b. These measurements confirm that the coupling to the

horizontal polarization is one order of magnitude smaller than to the vertical polarization.

2.3.6. Coupling Loop

Due to the reciprocity theorem the coupling from waveguide waves to the HOM absorber port corresponds to the coupling from this port to the waveguide waves. Therefore the DESY HOM coupler stimulates essentially horizontal polarized waves, while the SACLAY coupler stimulates vertical polarized waves although the orientation of the loops are very similar. A simple example is used to demonstrate that the polarization of excited waveguide waves is not necessarily determined by the loop orientation, but by the distribution of the current along the loop. The loop in Fig. 34 is symmetric with respect to the *u*-*v* and *u*-*w* planes. As both ends of the loop are connected to independent TEM ports, the current distribution is not fixed by an inner boundary condition (as for the DESY and SACLAY coupler). For a symmetric operation of both TEM ports, the current is symmetric to the *u*-*w* plane, and *u*-polarized H_{11} waves propagate in the positive and negative direction along the pipe as shown in Fig. 35. The *v*-polarized waves in Fig. 36 are caused by an anti-symmetric operation of the TEM ports. H_{11} waves with any direction of polarization and even any type of elliptical polarization are possible as a linear combination of these modes. Due to the *u*-*v* symmetry, the polarization is the same for the waves in both directions along the beam pipe. This is different for a loop with a tilt to the *u*-*w* plane.

2.4. Other Components

All components that are taken into account for the calculation of multi-cavity structures and complete modules can be seen in Fig. 37. The scattering parameters of the three types of cold windows (cf. Fig. 25) are shown in Fig. 38 and 39. As the reflection coefficient of the DESY-II window in the frequency range of the 3rd dipole band is very close to full reflection, all components beyond the window are neglected. This is different for the DESY-I and FNAL windows. Especially the FNAL window has a very broad frequency characteristic. This is related to the tapering angle of the conical window, which is 90^o minus the Brewster angle ($\arctan(\sqrt{\varepsilon_{\text{window}}/\varepsilon_0}) \approx 72^o$). Although the Brewster condition for the reflection-free transmission of plane waves through a plane surface is not exactly valid for conical objects the reflection from the window is quite small. The reflection coefficient in the reference plane between the main coupler six-port and the other components of the main coupler unit, as seen by the input coupler port, is shown in Fig. 40. This calculation includes the cold bellows (FNAL, DESY-II), the cold window, and for the DESY-I and FNAL main couplers the warm window, the warm bellows and the doorknob. The cold bellows on the inner conductor of the DESY-I main coupler is close to the tip of the coupling antenna and therefore discretized together with the main/HOM-coupler six-port. As the reflection coefficients of both DESY main couplers are large at the upper end of the 3rd dipole band, almost no HOM power is transmitted into the waveguide system and S parameter calculations are insensitive to boundary conditions behind the windows. The reflection from the FNAL window exhibits a more complicated frequency dependency and is considerably smaller in the frequency range between 2.57 and 2.6 GHz. The complicated frequency dependency is caused by the larger lengths of the waveguide components (to the warm window and its compensation elements) and by the stimulation of dipole modes in the coaxial line between the cold window and the doorknob. As several waveguide modes are above cutoff frequency it would be

extremely difficult to take into account further components such as three-stub-transformers and 3dB couplers. Therefore it is assumed for the following calculations that perfect loads terminate all waveguide modes. Due to this assumption the FNAL main coupler has a good capability to damp HOM modes at the upper end of the 3rd dipole band.

3. Test Cryostat

The performance of each TESLA cavity is routinely measured in two test cryostats: a vertical cryostat in which the input coupler flange is shorted and the so called CHECHIA cryostat. In both cryostats shorts terminate the beam pipes of the cavity as it can be seen in Fig. 41. As the vertical cryostat is used for the measurement of the internal quality of the superconducting cavities (~10^{10}), the main coupler is not assembled and its flange is also terminated by a conducting plane. For such measurements the HOM couplers are not connected to loads. In the CHECHIA cryostat the cavity is fully equipped with all couplers so that pulsed measurements of the accelerating mode ($Q_e \sim 10^6$) are possible. Fig. 42 shows the transmission between the two HOM ports of a cavity in the CHECHIA cryostat with a main coupler that is shorted after the cold window [18]. In this picture one can identify resonances of the 2nd monopole band, the 3rd dipole band and the second quadrupole band [8]. In the frequency range where the dipole band does not overlap with the quadrupole band, the characteristic double resonances of polarized dipole modes can be observed. One of the peaks of a double resonance is always much sharper than the other. This is a clear indication that the two polarizations of a dipole mode have very different quality factors. The frequency split of a double resonance has three sources: the polarization by the input coupler, the polarization by HOM couplers and the 'eigen'-polarization of the cavity due to perturbations of the axial symmetry. The polarizing effect of the input coupler depends (among other things) on the standing wave pattern along the coaxial line. It can be very strong if the coaxial line itself is close to a resonance condition.

3.1. Perfect Cavity

For simplicity the cavity-coupler-unit is calculated for an input coupler without inner conductor and shorted flange (cf. Fig. 41). This corresponds to the configuration in the vertical cryostat. The transmission between the HOM coupler ports of a cavity, which is equipped with DESY HOM couplers, is plotted in Fig. 43 for the full bandwidth of the 3rd dipole band. Fig. 44 shows the corresponding diagram for a cavity with SACLAY HOM couplers. For both cases a series of eight double resonances can be observed and one peak of a double resonance is always much sharper than the other. The double resonances with the highest frequencies for both coupler types are compared in Fig. 45. As DESY HOM couplers are much more effective for the horizontal than for the vertical polarization (cf. Fig. 28 and 29), the broader resonance is associated with a mode with essentially horizontal polarization and the sharp peak with one essentially vertically polarized. For similar reasons (cf. Fig. 30 and 31) this is otherwise for SACLAY HOM couplers. For both coupler types the lower resonance is related to the vertical and the higher resonance to the horizontal polarization.

The following method is used to calculate resonance frequencies ω_ν and quality factors Q_ν from complex transmission functions $s(\omega)$ with multiply overlapping

resonances: the transmission function $s(\omega)$ is fitted by a fractional function $\tilde{s}(\omega) = A(j\omega)/B(j\omega)$ with $A(p) = \sum a_\mu p^\mu$ and $B(p) = \sum b_\mu p^\mu$. The roots of the denominator function $B(p_\nu) = 0$ are the complex eigenvalues, which are related to ω_ν and Q_ν by $p_\nu = \omega_\nu\left(-1/(2Q_\nu) + j\right)$. Such a fit can be seen in Fig. 46 for the highest double resonance of a cavity with DESY HOM couplers. The resonance frequencies and quality factors are:

DESY	
f / GHz	Q / 1000
2.576971	3576
2.577146	18.2

SACLAY	
f / GHz	Q / 1000
2.577020	21.5
2.577122	2101

It is obvious that resonances with quality factors of the order 10^6 are possible in cavity-coupler units with ideal geometry. The mode polarization by the couplers causes a frequency split of 175 kHz for the DESY HOMCs and of 102 kHz for the SACLAY HOMCs.

3.2. Cavity with 'Eigen'-Polarization

To investigate the effect of the 'eigen'-polarization of a cavity with perturbed axial symmetry the cavity scattering matrix is approximated by Eq. 21. The resonance properties of the highest double resonance in a cavity-coupler unit with deformation parameters $\delta\omega_p = 2\pi\delta f$, $\delta\omega_q = 0$ and $\varphi = 0 \ldots \pi/2$ are calculated by the same method as described above. In Fig. 47 and 48 the quality factor is shown as a function of the polarization angle φ for a cavity with DESY and SACLAY HOM couplers respectively. It can be seen that the effect of the 'eigen'-polarization δf is negligible, if it is small compared to the frequency split of a perfect cavity due to the coupler polarization. However a large 'eigen'-polarization can cause the coupler damping to be more equally divided between both polarisations.

3.3. Modified HOM Coupler

As it was shown both (upstream and downstream) DESY type HOM couplers provide a very good coupling to the horizontal polarization while the coupling to the vertical polarization is one order of magnitude weaker although the orientation of the couplers is very different. The upstream and downstream SACLAY type couplers provide a very good coupling to the vertical but a much weaker coupling to the horizontal polarization. To achieve a better balance of the suppression of modes with different polarizations, we propose a symmetry transformation of the geometry of the upstream HOM coupler as shown in Fig. 49 for the DESY HOM coupler. This modification has several advantages: the modification is small, the location of the coupler flange is unchanged, the frequency characteristic is unchanged, the coupling to monopole modes is unchanged, the 1.3 GHz notch-filter still works, but the polarization of maximal coupling is rotated as it can be seen in the figure. Therefore the polarization of maximal coupling is now different for the upstream and downstream couplers. The same modification is proposed for the upstream SACLAY type coupler. Figs. 50 and 51 show the quality factor dependence on the polarization angle φ and the 'eigen'-polarization δf for a cavity with modified upstream HOM

couplers. In comparison to the original setup (see Figs. 47 and 48) the highest quality factors are reduced by one order of magnitude while the low Q factors are slightly increased.

4. Three-Cavity-Setups with Different Combinations of HOM Couplers

As it is mentioned in the introduction high Q dipole modes at the upper end of the 3rd band have been experimentally observed in the TTF modules 1, 2 and 3. The type of HOM and main couplers in these modules is described in the following table:

Module 1								
Cavity	D3	S8	S10	D1	D2	S11	D4	S7
FMC	FNAL	DESY-I	DESY-I	FNAL	FNAL	DESY-I	FNAL	FNAL
HOMC	DESY	SACLAY	SACLAY	DESY	DESY	SACLAY	DESY	SACLAY
Module 2								
Cavity	C22	C21	C25	C23	A15	C26	C27	C24
FMC	FNAL	FNAL	FNAL	FNAL	FNAL	FNAL	FNAL	FNAL
HOMC	SACLAY	SACLAY	SACLAY	SACLAY	DESY	SACLAY	SACLAY	SACLAY
Module 3								
cavity	D41	S32	S29	S30	D39	D40	S28	D42
FMC	DESY-II	DESY-II	DESY-II	DESY-II	DESY-II	DESY-II	DESY-II	DESY-II
HOMC	DESY	DESY	DESY	DESY	DESY	DESY	DESY	DESY

In the first two modules there are coupler-cavity units with DESY and SACLAY HOM couplers, which are efficient for different polarizations. So one expects that modes in the 3rd dipole band with any polarization are sufficiently damped, but experiments with intensity modulated beam and cold measurements gave a clear indication of high Q modes in the cavities S10, S11 and A15. Additionally it was found that the resonance frequencies of these cavities are approximately 10 to 20 MHz higher than that of their neighbors. Therefore there are resonances at the upper end of the 3rd dipole band which are trapped in these cavities. Only a small part of the field energy of these modes is stored in the end cells of the neigbouring cavities and the coupling to the rest of the module is negligible. To analyze the damping of these modes it is sufficient to consider three-cavity structures (cf. Fig. 37) with different types of main and HOM couplers. The scattering matrix of the middle cavity is shifted by 10 MHz to approximate the measured frequency shift, perfectly matched loads terminate the open beam pipe ends. The results of our calculations for different types of HOM and main couplers are summarized in the following table.

case	cavity 1 FMC HOMC	cavity 2 FMC HOMC $\Delta f = 10$ MHz	cavity 3 FMC HOMC	resonance frequency /GHz quality factor /1000 of the highest resonances			
S8,S10,D1 Figs. 52, 53	DESY-I SACLAY	DESY-I SACLAY	FNAL DESY	2.581504 6.94	2.581734 **441**	2.587299 31.1	2.587338 **2779**
D2,S11,D4 Figs. 54, 55	FNAL DESY	DESY-I SACLAY	FNAL DESY	2.582787 7.82	2.582896 19.4	2.587552 27.5	2.587557 **311**
C23,A15,C26 Figs. 56, 57	FNAL SACLAY	FNAL DESY	FNAL SACLAY	2.583486 47.9	2.584156 3.46	2.587745 **448**	2.587922 7.55
homogeneous DESY	DESY-II DESY	DESY-II DESY	DESY-II DESY	2.583467 **3160**	2.584121 5.19	2.587739 **1043**	2.588022 11.01
upstream HOM mirrored	DESY-II DESY	DESY-II DESY	DESY-II DESY	2.583348 21.7	2.584118 5.71	2.587746 74.8	2.588015 12.1

homogeneous SACLAY	FNAL SACLAY	FNAL SACLAY	FNAL SACLAY	2.583690 4.3	2.584312 9.77	2.587824 11.5	2.5882 19.65
upstream HOM mirrored	FNAL SACLAY	FNAL SACLAY	FNAL SACLAY	2.583748 5.55	2.584219 5.95	2.587830 15.1	2.588067 14.8

A configuration similar to that around cavity S10 in module 1 is considered in the first row of the table. Fig. 52 shows the transmission between the HOM couplers of the middle cavity for the whole frequency range of the 3rd dipole band. The resonance peaks below 2.58 GHz are very broad due to the absorption by the reflection free terminated beam pipes. As the middle cavity is shifted in frequency there are resonances above 2.58 GHz which hardly couple through the outer cavities. Therefore the last two double resonances above 2.58 GHz, which can also be seen in a magnified view in Fig. 53, are narrower. Their frequencies and quality factors are listed in the table. As for the case with SACLAY HOM couplers, see Fig. 45, the quality factor of the upper double resonance is much higher. These resonances are essentially horizontally polarized so that they have a weak coupling to the SACLAY HOM couplers of the middle cavity and to the downstream SACLAY HOM coupler of cavity 1. Only the upstream DESY HOM coupler of cavity 3 could be effective for these modes, but interference effects of forward and backward waves in the beam-pipe reduce its coupling. The dashed line in Fig. 53 is the transmission from the upstream HOM coupler of cavity 2 to the upstream HOM coupler of cavity 3. Indeed the upper double resonance couples better to the DESY HOM coupler than the lower one, but for the highest double resonance this coupling is still weaker than that to the SACLAY HOM coupler. The same behavior was observed in measurements (compare [5] Figs. 5.31 and 5.32).

The second row of the table describes a configuration similar to that around cavity S11 in module 1. There are two essential differences to the case of the first row: there are a DESY HOM coupler and a FNAL main coupler in the beam-pipe before cavity 2. Both couplers improve the damping of modes with horizontal polarization. Although the quality of the highest resonance is reduced by one order of magnitude it is still 311000.

All cavities in module 2 are equipped with FNAL main couplers and only cavity A15 has DESY HOM couplers. Therefore modes in cavity A15 with horizontal polarization are well damped. Only the lower mode of the highest double resonance is computed in our three-cavity-model with a quality factor of 448000. This mode is vertically polarized and therefore the SACLAY HOM couplers of the neighboring cavities could damp it, but interference effects in the beam pipes reduce this damping mechanism. The transmission between the HOM couplers of cavity 2 and the transmission from the upstream HOM coupler of cavity 2 to the upstream HOM coupler of cavity 3 are shown in Fig. 57. As in Fig. 45 for the case with DESY HOM couplers, the quality of the lower double resonance is much higher. The dashed curve in Fig. 57 with the transmission to the SACLAY HOM coupler confirms that the lower (vertically polarized) parts of double resonances have a better coupling than the upper parts, but this coupling is still weaker than that to the DESY HOM couplers.

The last four rows of the table consider three-cavity-models with homogeneous coupler equipment. In the case of cavities with DESY HOM and DESY-II main couplers the lower modes of the calculated double resonances have quality factors above 10^6 because these couplers damp only horizontally polarized modes. The situation is significantly better with modified upstream HOM couplers as proposed in section 3.3: the quality of the high Q modes is reduced to values below 10^5. In cavities

with SACLAY HOM couplers and FNAL main couplers all modes are sufficiently damped. The HOM couplers damp modes with vertical polarization while horizontally polarized modes couple through the main couplers. The HOM damping through the main coupler depends on boundary conditions (beyond the main coupler) that are not controlled by the design, and hence may change in the future. Therefore it is reasonable also to consider the case of cavities with modified SACLAY couplers as in the last row of the table.

5. Modules of Eight Cavity-Coupler Units

In this section we investigate an 8-cavity accelerating module corresponding to module 3, which contains 8 cavity-coupler units connected to each other by cylindrical bellows and terminated by infinitely long (matched) beam pipes at both (left and right) ends. Each cavity-coupler unit consists of a 9-cell cavity with a DESY type HOMC (see Fig.19) upstream and a DESY type HOMC+DESY-II FMC (see Figs. 23 and 25c) downstream. This accelerating module is simulated as a 16-port complex device and the 16×16 scattering matrix is calculated as a function of frequency. Each port corresponds to the coaxial output of a higher order mode coupler (8 upstream: port 1, 3, 5, 7, 9, 11, 13 and 15 and 8 downstream HOMCs: port 2, 4, 6, 8, 10, 12, 14 and 16). So we have the ability to study the dependence on frequency of any transmission coefficient $S_{ij}(f)$ and to investigate the resonance properties of each coupler-cavity unit or any combination of them.

We study seven cases of cavity detuning in the 8-cavity accelerating module. The detuning parameters are presented in the following table. There is no cavity detuning in Case 1; cavity 3 and cavity 7 have +10 MHz detuning in the Case 2, the other five cases correspond to random cavity detuning with uniform distribution from –10 MHz to +10 MHz (this is the range of cavity detuning which has been observed experimentally).

Case	Detunig of each cavity /MHz							
	cavity 1	cavity 2	cavity 3	cavity 4	cavity 5	cavity 6	cavity 7	cavity 8
1	0	0	0	0	0	0	0	0
2	0	0	**10**	0	0	0	**10**	0
3	2.539	-8.599	**4.916**	-9.625	-5.379	-4.895	**9.855**	-6.770
4	0.383	-3.889	-2.318	**7.110**	-2.638	3.244	-5.194	6.591
5	6.253	-7.767	**3.086**	-9.131	0.679	**9.263**	-1.822	4.283
6	-6.866	**9.594**	-3.372	**3.296**	**8.200**	**7.196**	**7.280**	-0.134
7	-8.314	**6.296**	-5.806	**9.994**	**3.978**	-5.765	-9.080	**8.698**

The simulation results are summarized in the next two tables. Cases 1-7 refer to the 8-cavity module with standard upstream coupler configration and Cases 1M-7M to the modules with modified upstream HOM couplers, as can be seen in Fig.49. All resonances are at the upper end of the 3rd dipole band except for those marked by (a) which correspond to resonances at the lower end.

Cases 1, 1M: First of all we studied an accelerating module with ideally tuned cavities in the frequency band corresponding to the upper end of the 3rd dipole passband. Simulations have shown that even in this ideal case there are some resonances with very high Q-factors in the frequency band from 2578 MHz to 2580 MHz. The simulation results were obtained from the frequency dependence of $S_{4,3}(f)$ (u2/d2 denotes the transmission between upstream and downstream HOMCs of the

second cavity-coupler unit). Modification of all upstream HOMCs strongly suppresses modes with high Q-factor (case 1M). For other cavity-coupler units we have obtained similar results (very high Q-factor at the upper end of the 3rd dipole passband), but of course the frequency dependence of the $S_{ij}(f)$ is then different.

Cases 2, 2M: in case 2 only two cavities were detuned. This case is approximately in agreement with the detuning of Module 3. The third and seventh cavities were detuned by +10 MHz while all other cavities were ideally tuned. The results presented in the table were obtained from the frequency dependence of $S_{6,5}(f)$ (third coupler-cavity unit, u3/d3) in the frequency band covering the two highest modes of the 3rd dipole band (from 2582 MHz to 2589 MHz). Very similar results were obtained for the 7th cavity-coupler unit, u7/d7.

Case	Resonance frequency /GHz Quality factor /1000 of resonances at the upper end of the 3rd band Cavity-coupler units: upstream HOMC (ui) / downstream HOMC (di)						
1			2.578295 71.5 u2/d2	2.578583 79.2 u2/d2	2.578820 **1138.2** u2/d2	2.578985 **287.2** u2/d2	2.579084 **530.0** u2/d2
1M			2.578291 31.1 u2/d2	2.578595 12.2 u2/d2	2.578806 44.4 u2/d2	2.578971 48.0 u2/d2	2.579072 52.7 u2/d2
2	(a) 2.474393 **3441.8** u4/d6	(a) 2.474816 **2222.2** u4/d6	(a) 2.475270 **1050.9** u4/d6	2.583471 **359.5** u3/d3	2.584129 4.88 u3/d3	2.587740 **1007.2** u3/d3	2.588024 11.0 u3/d3
2M	(a) 2.474426 53.7 u4/d6	(a) 2.474861 31.1 u4/d6	(a) 2.475326 22.5 u4/d6	2.583484 21.9 u3/d3	2.584116 6.0 u3/d3	2.587748 74.4 u3/d3	2.588017 12.2 u3/d3
3	2.579199 5.1 u3/d3	2.582706 **1062.8** u3/d3	2.582943 **335.2** u7/d7	2.583013 9.97 u3/d3	2.583610 4.8 u7/d7	2.587523 **1064.8** u7/d7	2.587792 11.4 u7/d7
3M	2.579168 6.0 u3/d3	2.582714 70.3 u3/d3	2.582968 20.6 u7/d7	2.583004 11.2 u3/d3	2.583583 5.9 u7/d7	2.587534 71.8 u7/d7	2.587781 13.0 u7/d7
4				2.580886 **348.2** u4/d4	2.581550 4.9 u4/d4	2.584921 **997.2** u4/d4	2.585227 10.3 u4/d4
4M				2.580894 21.9 u4/d4	2.581542 6.0 u4/d4	2.584928 72.8 u4/d4	2.585221 11.3 u4/d4
5		2.580965 **1049.0** u3/d3	2.581294 9.5 u3/d3	2.582837 **334.4** u6/d6	2.583503 4.8 u6/d6	2.587018 **987.3** u6/d6	2.587302 11.0 u6/d6
5M		2.580971 70.1 u3/d3	2.581288 10.4 u3/d3	2.582847 21.9 u6/d6	2.583492 5.9 u6/d6	2.587026 72.1 u6/d6	2.587294 12.2 u6/d6

(a) corresponds to resonances at the lower end of the 3rd dipole band.

At the same time modes with very high Q-factors were observed in the lower frequency band of the 3rd dipole band. The table presents data obtained with $S_{12,7}(f)$ dependence on frequency (upstream HOMC of the 4th cavity-coupler unit and downstream of the 6th, u4/d6) in the frequency band 2473 – 2478 MHz. These data are marked by (a) in the table.

This detuning causes weak coupling to some of the HOM couplers due to the standing wave pattern in the beam pipes. Measurements with intensity modulated beam and network analyzer [5,6,7] showed high Q-factor resonances at the upper end of the 3rd dipole band for the 7th and 3rd cavity-coupler units of module 3. At the same time a detuning of about +10 MHz was observed. This means that the neighbouring cavities create a full reflection at frequencies of about 2590 MHz. As the DESY type HOMC provides very weak coupling to the vertical polarization, high Q-factor resonances of the vertically polarized modes are observed. Our simulation of this condition shows that high Q-factor resonances are observed at the upper end of the 3rd dipole band for the 3rd and 7th cavity-coupler units. The high Q-factor resonances in the lower frequency range of the 3rd dipole band can be explained by the total reflection in the 3rd and 7th units and by the fact that the system of three cavity-coupler units (4th, 5th and 6th) is terminated by the fully reflecting 3rd (on the left side) and 7th cavity-coupler units (on the right side).

One can see strong suppression of all higher Q-factor modes due to the modification of all upstream HOMCs (Case 2M).

Cases 3-7 and, 3M-7M present simulations of random detuning of the cavities. We used detuning with the same uniform frequency distribution for both polarizations in the frequency range ±10 MHz. Investigations were carried out in the frequency range from 2579 MHz to 2589 MHz with different combinations of ports for $S_{i,j}(f)$.

Cases 3, 3M: Data was obtained from the frequency dependence of $S_{14,13}(f)$ and $S_{6,5}(f)$ (u7/d7 and u3/d3). These transmission coefficients, $S_{14,13}(f)$ and $S_{6,5}(f)$, correspond to upstream and downstream HOMCs of the seventh and third cavity-coupler units respectively. Cavities of these units have the largest positive detuning. The data for *Case 4* was obtained from $S_{8,7}(f)$ (fourth cavity-coupler unit, u4/d4). Data for *Case 5* was obtained from $S_{12,11}(f)$ and $S_{6,5}(f)$ (sixth and third cavity-coupler unit, u6/d6 and u3/d3). These three random samples have common features: the cavities with the largest positive detuning have neighbouring cavities with negative or little positive detuning. In all these cases one can see strong suppression of the modes with the largest Q-factor due to the modification of all upstream HOMCs.

Cases 6, 6M and 7, 7M have more complicated frequency properties. In Case 6 the second cavity has the largest positive detuning and the neighbouring cavities have negative detuning. Cavities 4 - 7 have similar positive detunings. In Case 7 cavities have detuning with an average value of less than 10^{-6} MHz.

The next table presents resonance frequencies and Q-factors obtained from the frequency dependence of the transmission coefficients in the frequency range from 2579 MHz to 2589 MHz (case 6 and 6M). In the cases 7 and 7M cavity-coupler units 2, 4 and 5 (u2/d2, u4/d4, u5/d5) have the largest Q-factors in the same frequency range. The entries are arranged in order of ascending frequency for the calculation of Cases 6 and 7, with the corresponding calculation for the mirrored cases, 6M and 7M, in the adjacent column.

Some modes presented in this table occur with very similar frequencies but with HOMCs of different cavity-coupler units. These sets of corresponding modes are indicated by the superscripts 1 to 6. Slight differences in frequency or in Q-factor may be due to numerical error.

Resonance frequency /GHz; Quality factor /1000 of resonances at the upper end of the 3rd band (Cavity-coupler unit Upstream HOMC ui/ Cavity-coupler unit Downstream HOMC di)			
Case 6	Case 6M	Case 6 (continued)	Case 6M (continued)
2.579512; **227.0** (u4/d4)[1]	2.579527; 20.0 (u4/d4)	2.583029; **439.8** (u4/d4)[4]	2.583017; 29.9 (u4/d4)
2.579513; **198.1** (u5/d5)[1]	2.589525; 20.9 (u5/d5)	2.583029; **337.5** (u6/d6)[4]	2.583017; 26.5 (u6/d6)
2.579512; **208.2** (u6/d6)[1]	2.579529; 22.6 (u6/d6)	2.583029; **339.1** (u7/d7)[4]	2.583016; 26.3 (u7/d7)
2.579513; **209.6** (u7/d7)[1]	2.579528; 23.8 (u7/d7)	2.583124; **335.0** (u5/d5)	2.583017; 6.1 (u5/d5)
2.580042; 6.0 (u6/d6)	2.580023; 7.4 (u6/d6)	2.583437; 4.8 (u2/d2)	2.583414; 6.0 (u2/d2)
2.580042; 5.8 (u7/d7)	2.580021; 7.3 (u7/d7)	2.583609; 10.8 (u7/d7)	2.583705; 6.1 (u7/d7)
2.580043; 6.3 (u5/d5)	2.580030; 7.4 (u5/d5)	2.583666; 4.7 (u4/d4)	2.583685; 5.8 (u4/d4)
2.580068; 6.7 (u4/d4)	2.580038; 7.8 (u4/d4)	2.583691; 5.1 (u6/d6)	2.583703; 6.2 (u6/d6)
2.580874; **420.2** (u4/d4)[2]	2.580883; 37.3 (u4/d4)	2.583692; 5.2 (u5/d5)	2.583703; 26.9 (u5/d5)
2.580874; **449.3** (u5/d5)[2]	2.580885; 35.1 (u5/d5)	2.584788; **736.2** (u6/d6)[5]	2.584795; 71.0 (u6/d6)
2.580874; **451.6** (u6/d6)[2]	2.581096; 9.5 (u6/d6)	2.584788; **745.6** (u7/d7)[5]	2.584795; 71.6 (u7/d7)
2.580874; **443.5** (u7/d7)[2]	2580884; 36.4 (u7/d7)	2.584816; 20.8 (u5/d5)	2.584794; 73.0 (u5/d5)
2.581270; 7.8 (u4/d4)	2.581260; 9.2 (u4/d4)	2.585094; 10.0 (u6/d6)	2.585088; 10.7 (u6/d6)
2.581268; 8.0 (u5/d5)	2.581267; 9.5 (u5/d5)	2.585094; 10.0 (u7/d7)	2.585088; 10.7 (u7/d7)
2.581272; 4.0 (u6/d6)	2.581134; 7.0 (u6/d6)	2.585558; **703.2** (u6/d6)[6]	2.585556; 60.9 (u6/d6)
2.581271; 8.0 (u7/d7)	2.581261; 9.4 (u7/d7)	2.585558; **705.0** (u7/d7)[6]	2.585559; 61.2 (u7/d7)
2.581758; **375.7** (u4/d4)[3]	2.581755; 31.4 (u4/d4)	2.585909; 8.9 (u6/d6)	2.585912; 9.9 (u6/d6)
2.581757; **403.3** (u5/d5)[3]	2.581766; 28.9 (u5/d5)	2.585908; 9.0 (u7/d7)	2.585912; 9.9 (u7/d7)
2.581757; **395.2** (u6/d6)[3]	2.581756; 29.3 (u6/d6)	2.586013; 0.6 (u5/d5)	2.586002; 7.6 (u5/d5)
2.581757; **399.4** (u7/d7)[3]	2.581755; 29.9 (u7/d7)	2.586373; **812.2** (u5/d5)	2.586371; 70.5 (u5/d5)
2.582266; 6.0 (u4/d4)	2.582.267; 7.5 (u4/d4)	2.586373; **809.1** (u6/d6)	2.586370; 71.9 (u6/d6)
2.582275; 5.9 (u5/d5)	2.582273; 7.8 (u5/d5)	2.586731; 8.9 (u5/d5)	2.586736; 9.8 (u5/d5)
2.582274; 6.4 (u6/d6)	2.582272; 7.9 (u6/d6)	2.586731; 8.8 (u6/d6)	2.586734; 9.6 (u6/d6)
2.582274; 6.3 (u7/d7)	2.58272; 7.8 (u7/d7)	2.587287; **1076.6** (u2/d2)	2.587296; 75.1 (u2/d2)
2.582768; **339.3** (u2/d2)	2.582791; 21.3 (u2/d2)	2.587568; 11.1 (u2/d2)	2.587559; 12.4 (u2/d2)
Case 7	Case 7M	Case 7 (continued)	Case 7M (continued)
2.579823; **355.7** (u2/d2)	2.579839; 21.3 (u2/d2)	2.583618; **328.8** (u5/d5)	2.583620; 19.3 (u5/d5)
2.580493; 4.8 (u2/d2)	2.580475; 6.0 (u2/d2)	2.584072; **1067.2** (u2/d2)	2.584080; 73.7 (u2/d2)
2.581654; **1127.3** (u4/d4)	2.581666; 64.4 (u4/d4)	2.584216; 4.3 (u5/d5)	2.584197; 5.6 (u5/d5)
2.581654; **854.0** (u5/d5)	2.581664; 64.9 (u5/d5)	2584217; 5.3 (u4/d4)	2.584206; 6.7 (u4/d4)
2582048; 8.3 (u5/d5)	2.582040; 8.9 (u5/d5)	2.584379; 10.3 (u2/d2)	2.584371; 11.3 (u2/d2)
2.582051; 9.1 (u4/d4)	2.582040; 9.7 (u4/d4)	2.587759; **1040.5** (u4/d4)	2.587765; 80.5 (u4/d4)
2.583618; **345.3** (u4/d4)	2.583627; 23.0 (u4/d4)	2.588067; 10.4 (u4/d4)	2.588063; 11.3 (u4/d4)

Superscripts 1, 2, 3, 4, 5 or 6 indicate sets of corresponding modes.

Analysis of the data presented in this section shows that even in the ideal case there are some resonances with very high Q-factors. Detuning of the cavities (fixed or random) can cause some resonances with very high Q-factors. In all cases modification of all upstream higher order mode couplers creates very strong suppression of high Q-factor modes and very little increase in those with low Q-factors.

6. First and Second Dipole Band

We used the same method as described above to compute the quality factors of dipole modes in the 1st and 2nd band. The calculation is significantly simplified because these modes are below the cutoff frequency of the beam-pipe, so that only a single cavity-coupler unit has to be considered. Additionally we neglect the main coupler and use only the 5-port scattering matrix of the HOM coupler. The scattering matrices of the couplers on both sides as well as the matrix of the modified (mirrored) coupler are related to each other by rotation and mirror transformations. Therefore the scattering matrix of the DESY and SACLAY HOM couplers only have to be calculated for a single orientation.

In Figs. 58 and 59 the calculated and measured [18] quality factors of cavities with DESY and SACLAY HOM couplers are compared. For each mode, two quality factors are computed which correspond to both polarizations. The modes with the largest loss-parameters are in the index range from 4 to 15 (cf. Fig. 16), the modes 6, 7, 13 and 14 are especially important.

The calculated quality factors of a cavity with standard DESY HOM couplers and a modified upstream coupler (cf. Fig. 22) are shown in Fig. 60. For the standard coupler setup and modes of the 1st band (modes 1 to 9), the Q values of modes with different polarization (but with the same mode number) are quite close to each other. For this band the azimuthal orientation of the couplers is nearly optimal. The quality factors of modes in the 2nd band (modes 10 to 18) of both polarizations deviate by more than a factor 2.5 from each other. The frequency behavior of the Q values of a cavity with modified upstream coupler is similar to that of the original setup, but the Q values of modes with the same number differ approximately by a factor 2.2 for both bands. An optimal performance with respect to the polarization could be achieved with a modified upstream coupler that is azimuthally orthogonal to the downstream coupler. For this case the slight asymmetry of the damping of both polarizations is caused by the length-asymmetry of the cavity. A disadvantage of the setup with the orthogonal modified coupler is that one polarization of quadrupole modes is nearly undamped.

Fig. 61 shows the quality factors of a cavity with original, modified and modified orthogonal SACLAY HOM couplers. The performance of the cavity with modified upstream coupler is very similar or even better than that of the original setup. In a cavity with orthogonal modified couplers the quality factors of modes with different polarization are quite close to each other.

7. Conclusion and Outlook

The damping mechanisms of modes in the frequency range of the 3rd dipole band were quantitatively analyzed with the method of coupled scattering parameters. We could identify two main reasons for the very weak damping of some modes in this frequency range.

1) Due to their design DESY type couplers are insensitive to vertically polarized modes and SACLAY type couplers have a weak coupling to modes with horizontal polarization. 2) Interference effects of forward and backward waves in the beam pipe can reduce the coupling.

We have shown that the measured high Q modes are in agreement with the numerical model. The coupling of upstream and downstream HOM couplers to nearly the same

polarization and the missing coupling to perpendicularly polarized modes is a design problem which can be avoided by another azimuthal position or another shape of the couplers. We propose to keep the position of the couplers and to change the orientation of the coupling loop in the upstream coupler. As the interference effect depends on the random differences between the cavities it is practically impossible to avoid the cancellation of coupling fields in general. Therefore the number of HOM couplers has to be large enough so that the damping is sufficient even if some couplers are ineffective. It is shown for several arrangements of systematically and randomly detuned cavities with modified upstream HOM couplers that the highest quality factors of modes in the 3rd dipole band are always below 10^5. The quality factors of dipole modes in the 1st and 2nd band are similar as with the existing arrangement.

Further investigations are still necessary. Other modifications of the HOM couplers such as different azimuthal orientations and a modified orientation of the coupling loop for the upstream and/or downstream coupler should be considered. Better models of the detuned cavities need to be developed, based on shape deformations [19] and possibly on a perturbation of the symmetry of revolution. In addition the calculation of more random samples is needed.

8. Acknowledgement

We would like to thank N.Baboi, C.Magne, H.-W.Glock, K.Rothemund, U. van Rienen, W.Müller, T.Weiland, O.Napoly, R.Wanzenberg, R.Brinkmann, J.Sekutovicz, G. Kreps and D.Proch for many useful discussions.

References

[1] D.A.Edwards (ed.): TESLA Test Facility Linac - Design Report, DESY TESLA-95-01, 1995.

[2] R.Brinkmann, G.Materlik, J.Rossbach and A.Wagener (eds.): Conceptual Design of a 500 GeV e+e- Collider with Integrated X-ray Laser Facility, DESY-97-048 and ECFA-97-182.

[3] R.Brinkmann, K.Flöttmann, J.Rossbach, P.Schmüser, N.Walker, H.Weise (eds.): TESLA The Superconducting Electron-Positron Linear Collider with an Integrated X-Ray Laser Laboratory, Technical Design Report, Part II The Accelerator, DESY 2001-011, ECFA 2001-209, TESLA Report 2001-23, TESLA-FEL 2001-05.

[4] S.Farthoukh, et al.: Evidence for a Strongly Coupled Dipole Mode with Insufficient Damping in TTF First Accelerating Module, Proc. 18th Particle Accelerator Conference (PAC99), p922, New York, March/April 1999.

[5] N.Baboi: Studies on Higher Order Modes on Accelerating Structures for Linear Colliders, PHD thesis University of Hamburg, Hamburg 2001

[6] C.Magne, M.Jablonka, M.Lalot, V.Lethiers, M.Luong, O.Napoly, N.Baboi, P.Castro, A.Gossel, M.Huning, G.Kreps, M.Liepe, M.Minty, S.Schreiber, D.Sertore, M.Wendt: Measurement with Beam of the Deflecting Higher Order Modes in the TTF Superconducting Cavities, Proc. 20th Particle Accelerator Conference (PAC2001), Chicago, June 2001.

[7] N.Baboi, M.Dohlus, C.Magne, A.Mosnier, O.Napoli, H.-W.Glock: Investigation of High-Q Dipole Mode at the TESLA Cavities, Proc. 7th European Particle Accelerator Conference (EPAC2000), pp. 1107, June 2000.

[8] R.Wanzenberg: Monopole, Dipole and Quadrupole Passbands of the TESLA 9-cell Cavity, TESLA 2001-33, 2001.

[9] T.A.Abele: Über die Streumatrix allgemein zusammengeschalteter Mehrpole, Arch. El. Übertrag., 1960, Bd 14, No 6, pp. 161-168.

[10] M.A.Silaev, C.F.Bryantsev: Use of Matrix for Investigation of Microwave Devices (in Russian), Sovetskoye Radio, Moscow, 1970, pp. 30-49.

[11] M.Dohlus, R.Schuhmann, T.Weiland: Calculation of Frequency Domain Parameters usind 3D Eigensolutions, International Journal of Numerical Modelling, Electronic Networks, Devices and Fields, Vol. 12, Number 1/2, pp. 81-92, Jan. - April 1999.

[12] The MAFIA Collaboration, MAFIA Manual Version 4.00, CST GmbH, Lautenschlägerstr. 38, 64289 Darmstadt, Germany 1997.

[13] M.Dohlus, H.-W.Glock, D.Hecht, U.v.Rienen: Filling and Beam Loading in TESLA Superstructures, TESLA 98-14, 1998.

[14] H.-W.Glock: private communication, 1998.

[15] T.Weiland, R.Wanzenberg: Wake Fields and Impedances, in: Joint US-Cern part. acc. school, Hilton Head Island, SC, USA, 7-14 Nov. 1990 / Ed. By. M. Dienes,

M. Month and S. Turner, Springer, Berlin, 1992- (Lecture notes in physics; 400) pp. 39-79.

[16] CST GmbH, Lautenschlägerstr. 38, 64289 Darmstadt.

[17] M.Dohlus, S.Wipf: Numerical Investigation of Waveguide Input Couplers for the TESLA Superstructure, DESY-M-00-04X, Nov. 2000.

[18] G.Kreps: private communication.

[19] W.Koch: Numerische Simulation der Abstimmprozedur von Beschleuniger-resonatoren für TESLA, Entwicklung eines Ersatzkreismodels, Studienarbeit, TU-Darmstadt, Fachgebiet TEMF, Mar. – Aug. 2001

Figures

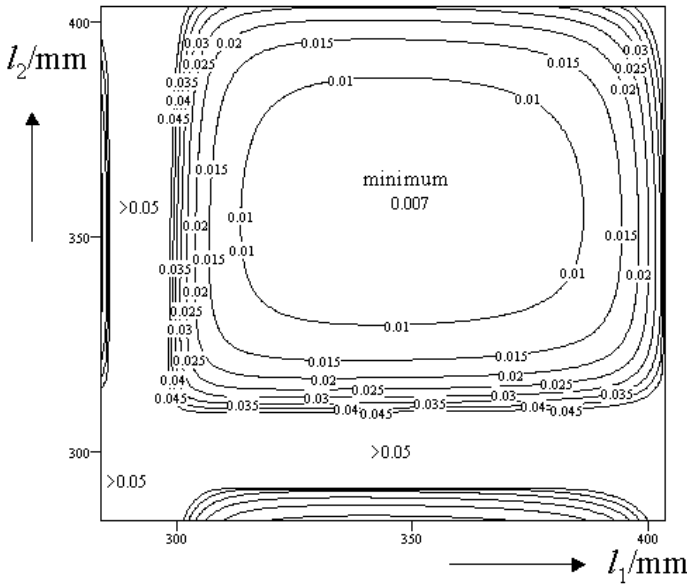

Fig. 1: Ratio $X = W_{\text{tot}}/W_{\text{pipe}}$ in the two dimensional parameter range $l_{\text{pipe}} - \lambda/4 \le l_{1/2} \le l_{\text{pipe}} + \lambda/4$ with $l_{\text{pipe}} = 0.344\,\text{m}$, $\lambda = 0.24\,\text{m}$.

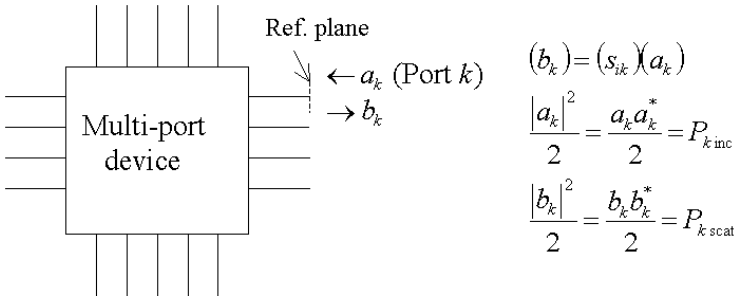

Fig. 2. Multi-port device and its normalized scattering-matrix.

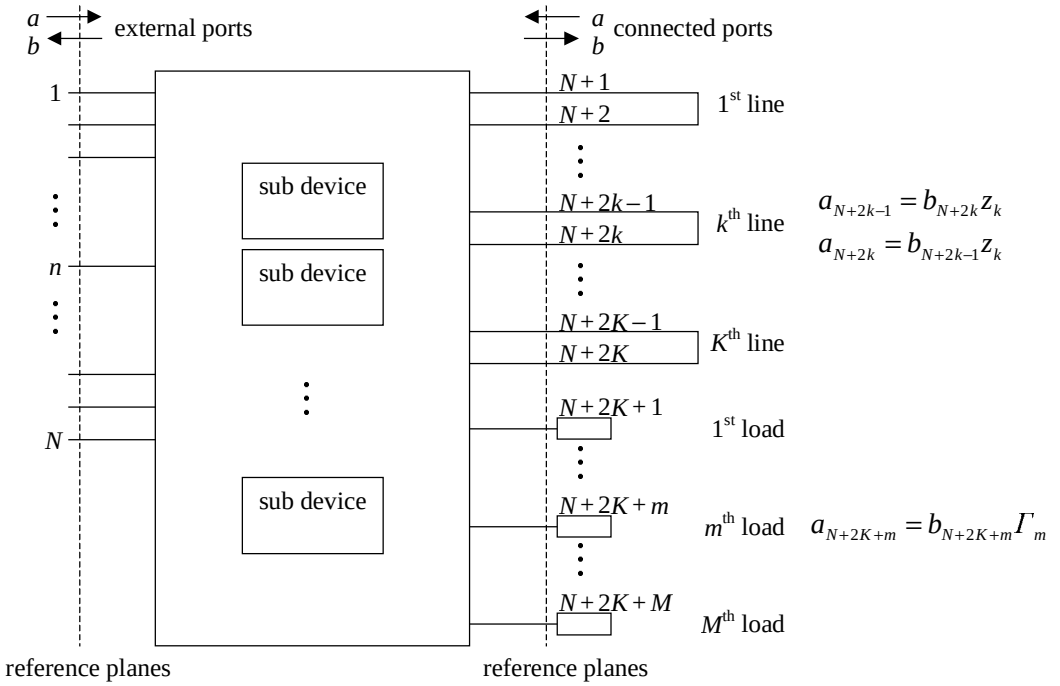

Fig. 3. Port connection of a system which is composed of several sub devices.

Fig. 4: Photo of the TESLA nine cell cavity with welded HOM couplers.

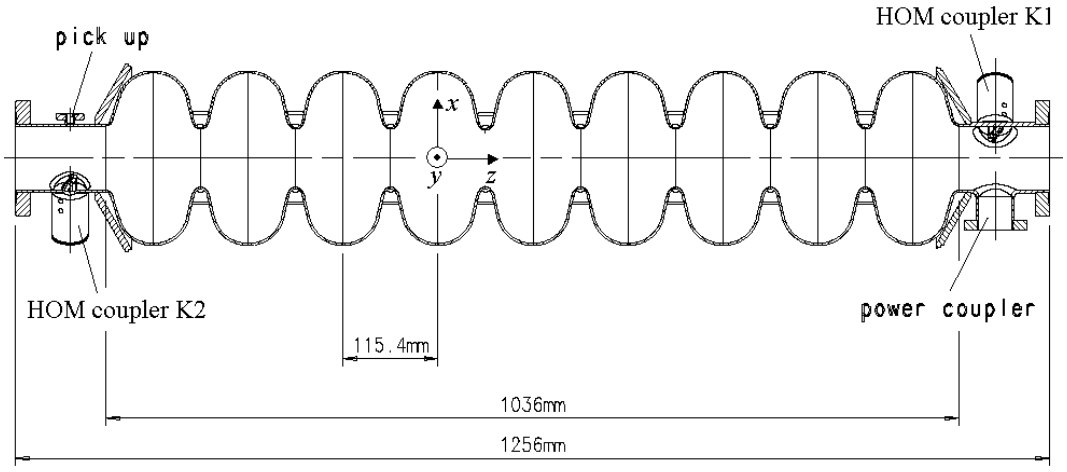

Fig. 5: Design of the TESLA cavity. The cavity is positioned in the modules such the beam comes from left. When viewed from the right end, the HOM couplers make with the power coupler angles of 145^{o} (K1) and 30^{o} (K2). The *x*-*z* plane is the horizontal plane.

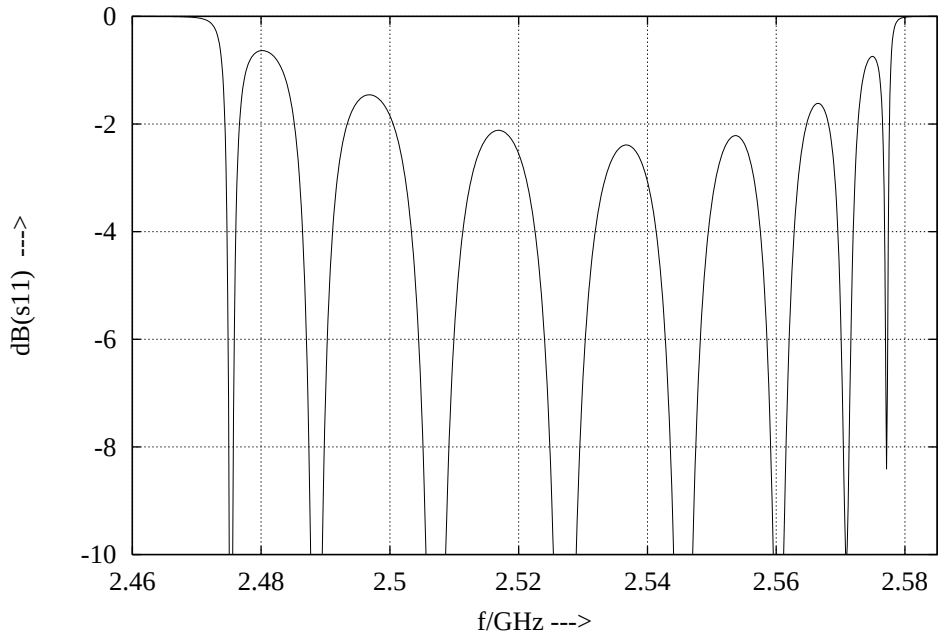

Fig. 6: Amplitude in dB of the reflection coefficient s_{11} of a TESLA cavity.

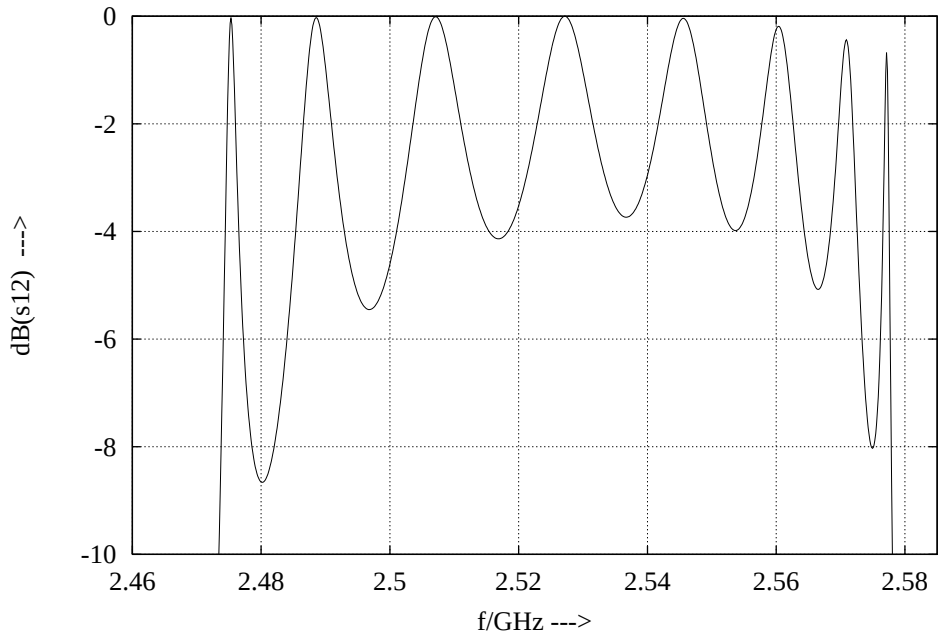

Fig. 7: Amplitude in dB of the transmission coefficient s_{12} of a TESLA cavity.

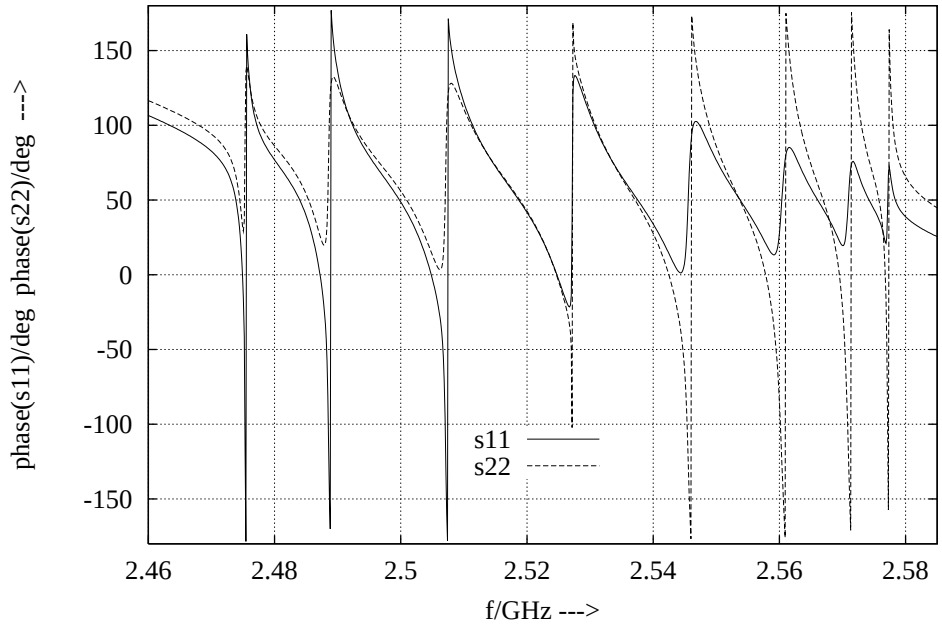

Fig. 8: Phase in deg. of the reflection coefficients s_{11}, s_{22} of a TESLA cavity. The lengths of the beam pipes on both sides are 100 mm.

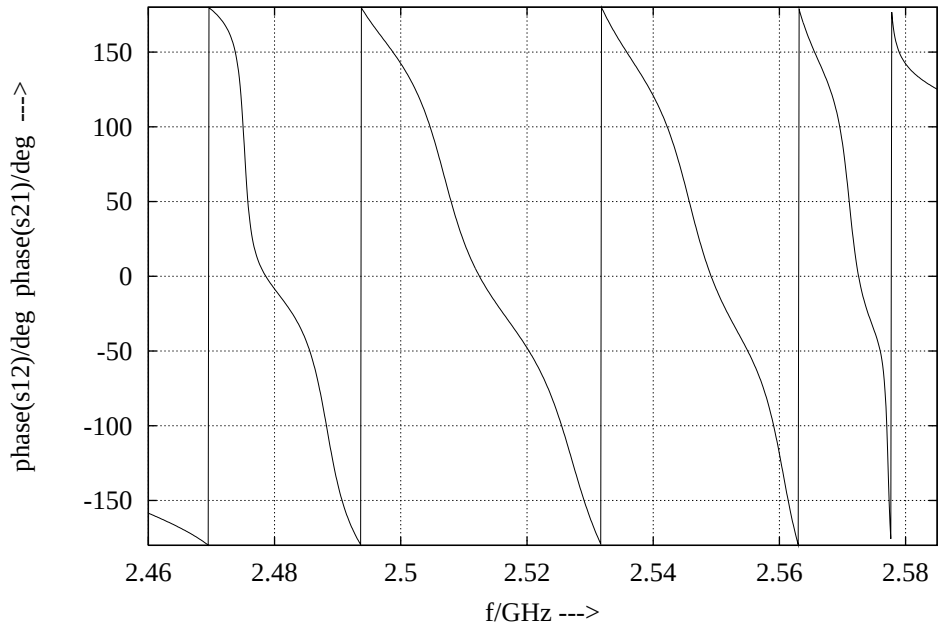

Fig. 9: Phase in deg. of the transmission coefficients s_{12} of a TESLA cavity. The lengths of the beam pipes on both sides are 100 mm.

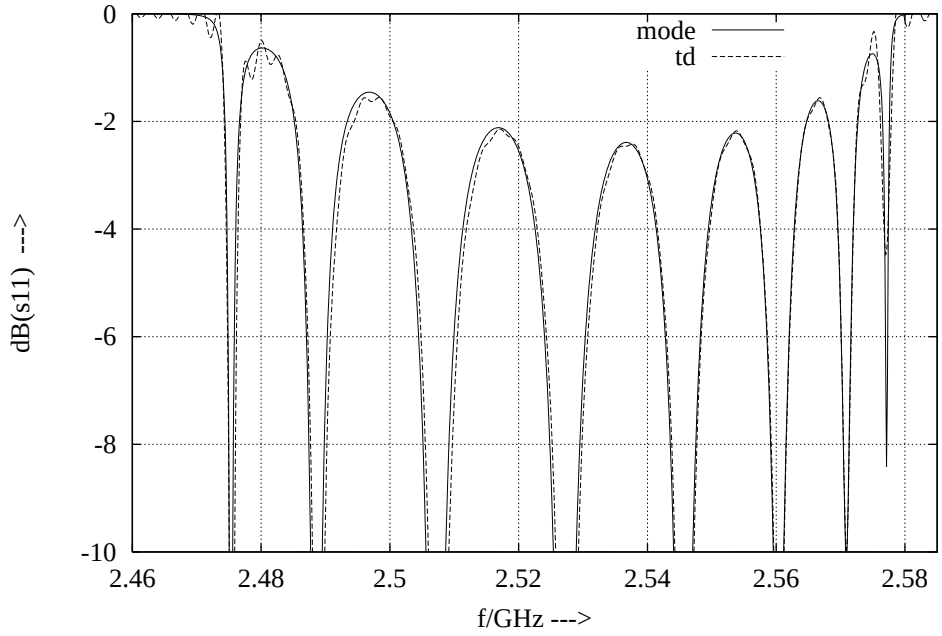

Fig. 10: Comparison of a modal and a time domain (td) calculation: Amplitude in dB of the reflection coefficient s_{11} of a TESLA cavity.

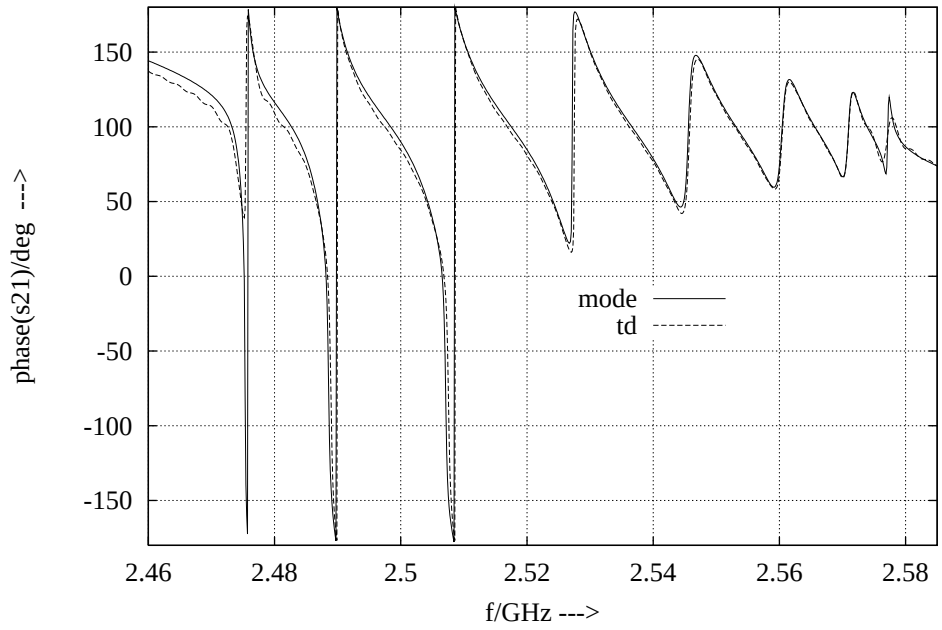

Fig. 11: Comparison of a modal and a time domain (td) calculation: Phase in deg. of the transmission coefficients s_{11} of a TESLA cavity. The length of the left beam pipe is 84.15 mm, the length of the right beam pipe is 86.51 mm.

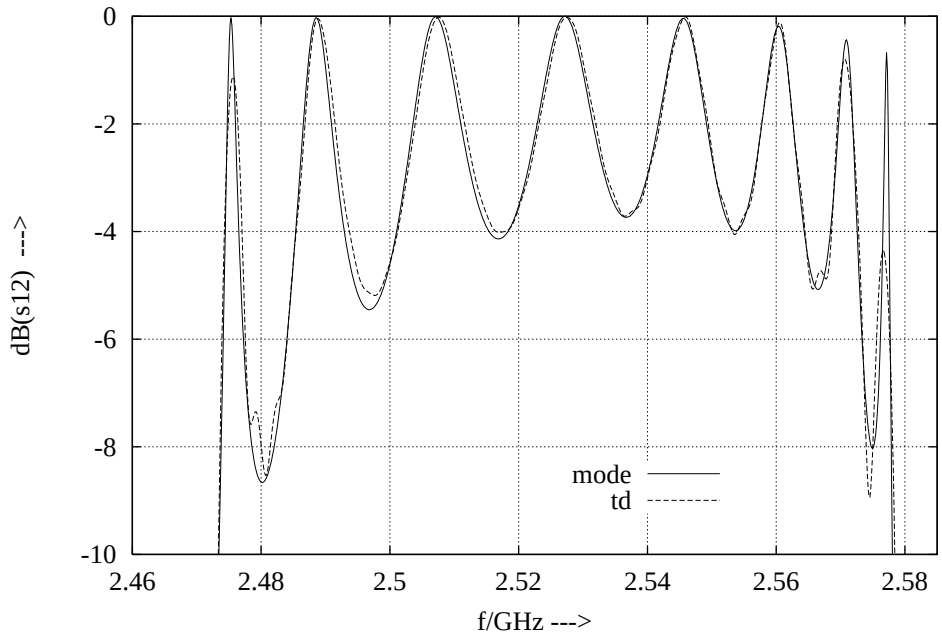

Fig. 12: Comparison of a modal and a time domain (td) calculation: Amplitude in dB of the transmission coefficient s_{21} of a TESLA cavity.

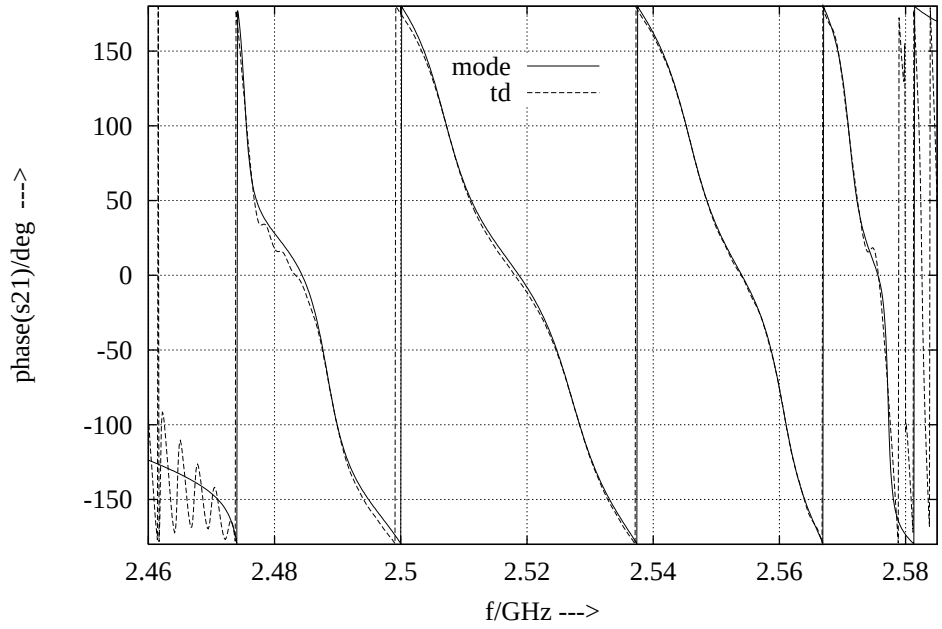

Fig. 13: Comparison of a modal and a time domain (td) calculation: Phase in deg. of the transmission coefficients s_{21} of a TESLA cavity. The length of the left beam pipe is 84.15 mm, the length of the right beam pipe is 86.51 mm.

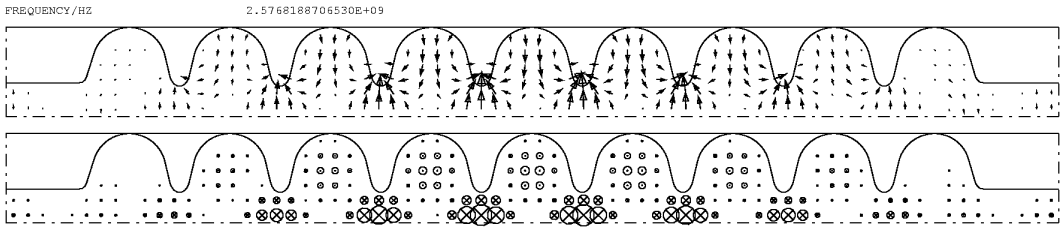

Fig. 14: Electric field of the 28th mode in the TESLA cavity (left beam pipe 84.15 mm, right beam pipe 86.51 mm, magnetic boundary conditions, $f = 2.576819$ GHz). The upper part of the picture shows the plane with pure longitudinal and radial field components, the lower part shows the azimuthal component in the perpendicular plane.

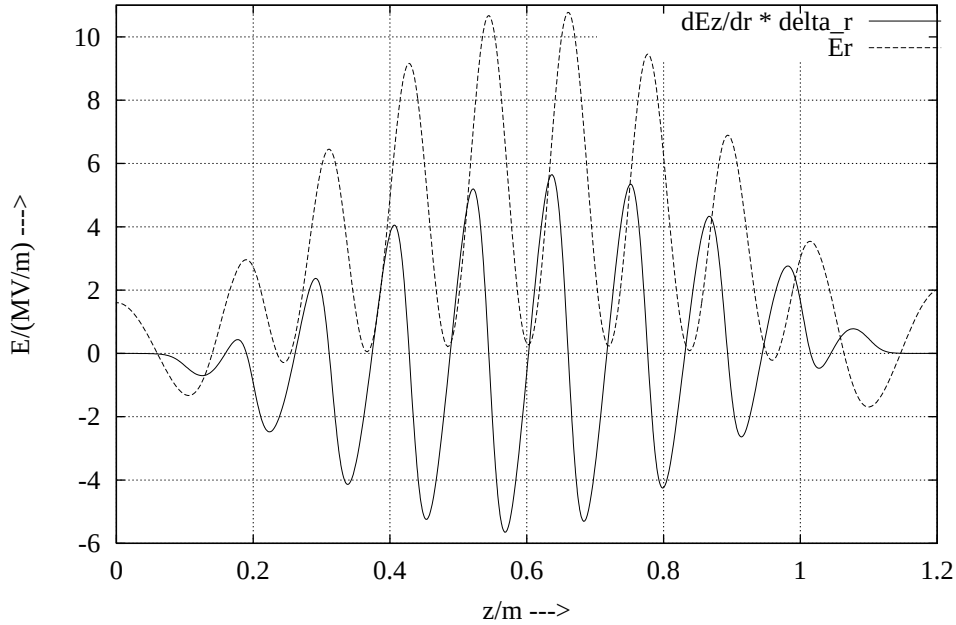

Fig. 15: Radial electrical field E_r and derivative of the longitudinal field $\partial E_z / \partial r$ on the cavity axis for the 28th mode ($\Delta r = 3$ cm, left beam pipe 84.15 mm, right beam pipe 86.51 mm, magnetic boundary conditions, f = 2.576819 GHz). The total field energy of this mode is normalized to 1 J.

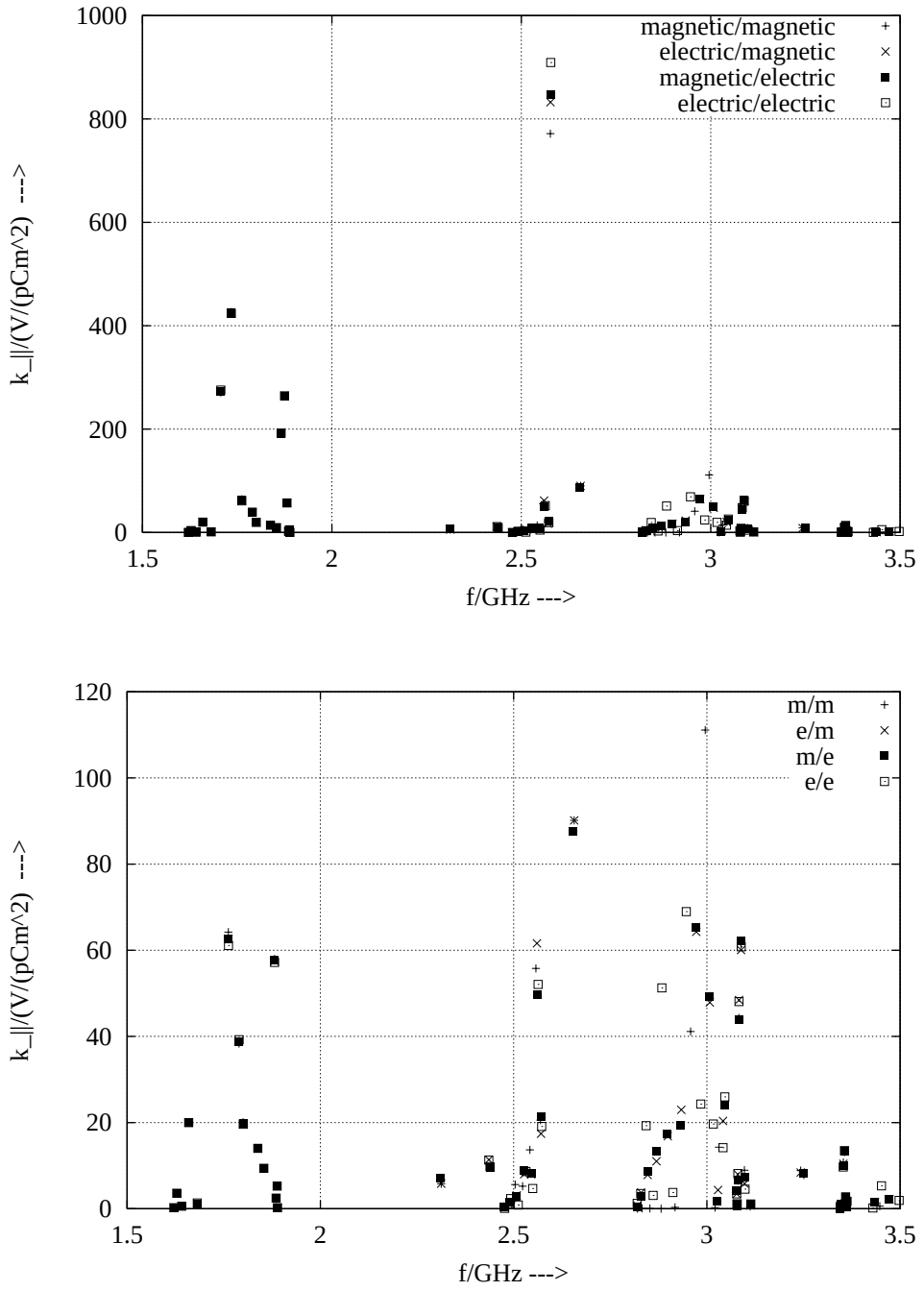

Fig. 16: Dipole loss parameters for different boundary conditions (left beam pipe 84.15 mm, right beam pipe 86.51 mm). The upper diagram shows the full ordinate range while the ordinate scale in the lower diagram is expanded.

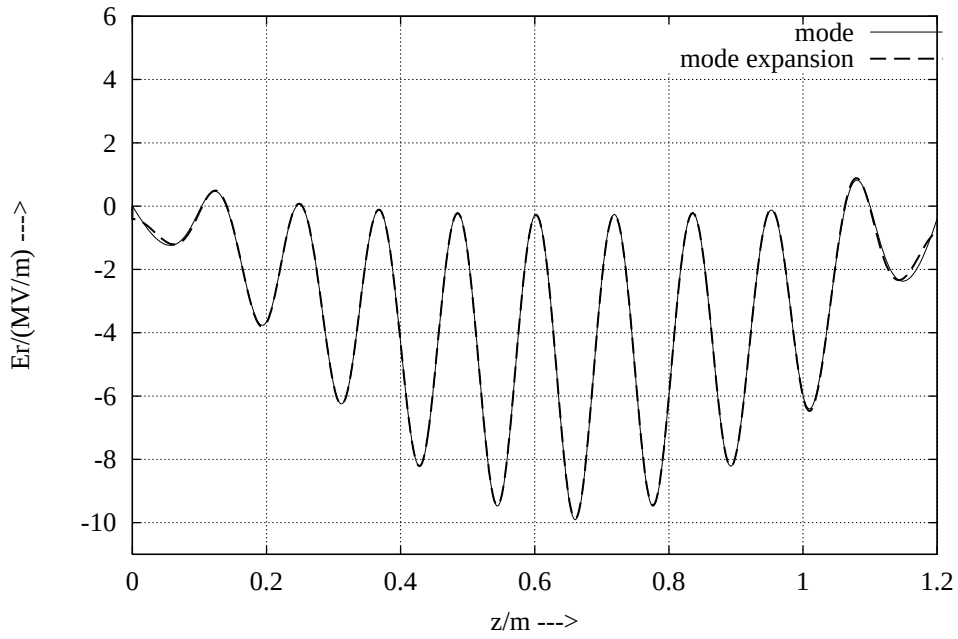

Fig. 17: Comparison direct mode calculation for electric boundary conditions and mode expansion by modes calculated for magnetic boundary conditions. Radial electrical field E_r for the 28th mode (left beam pipe 84.15 mm, right beam pipe 86.51 mm, magnetic boundary conditions, $f = 2.577657$ GHz, total field energy 1 J).

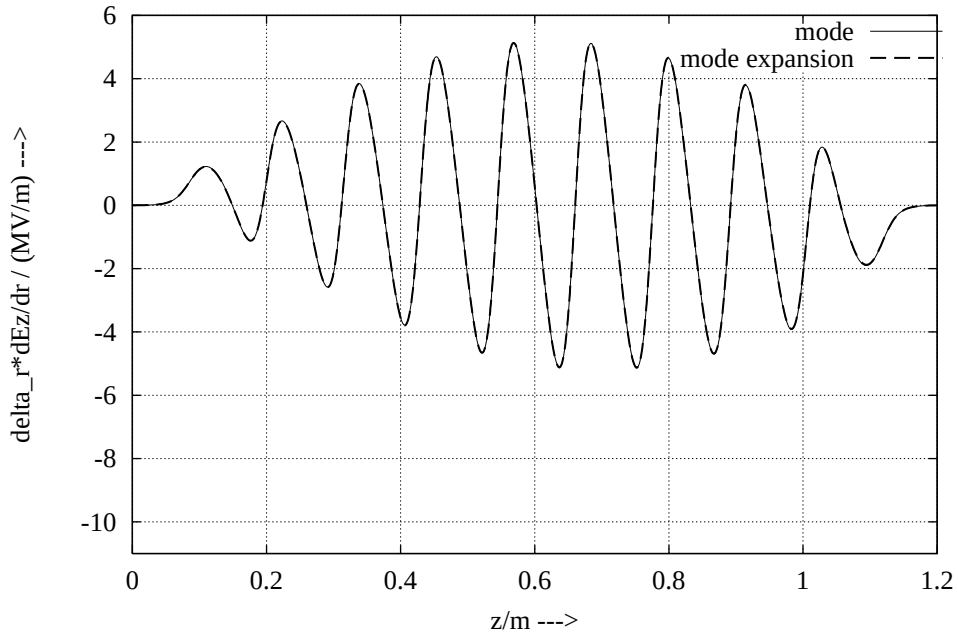

Fig. 18: Same comparison as for Fig. 17, but for $\Delta r \cdot \partial E_z / \partial r$ with $\Delta r = 3$ cm.

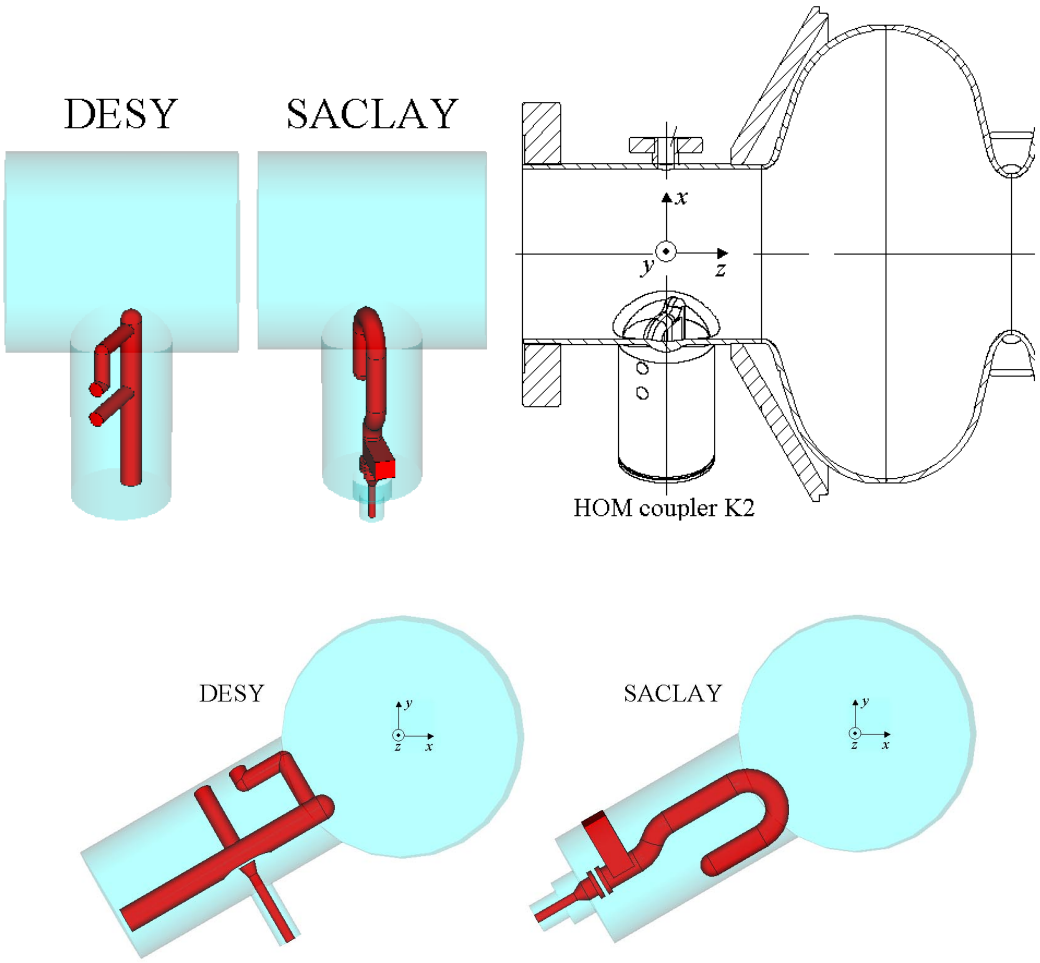

Fig. 19: Orientation of the upstream HOM coupler (*x* is the horizontal coordinate, *z* is the direction of the beam). The angle between the horizontal axis and the axis of the HOM cylinder is -150^{o}.

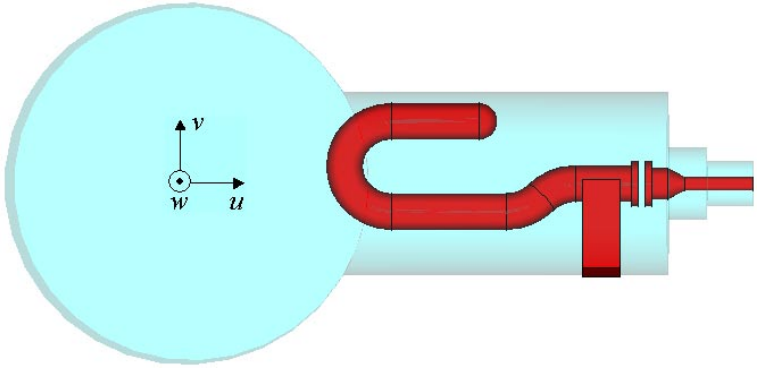

Fig. 20: Coordinate system of the rectangular *u*,*v*,*w* mesh which is used for the discretization of both coupler types (upstream).

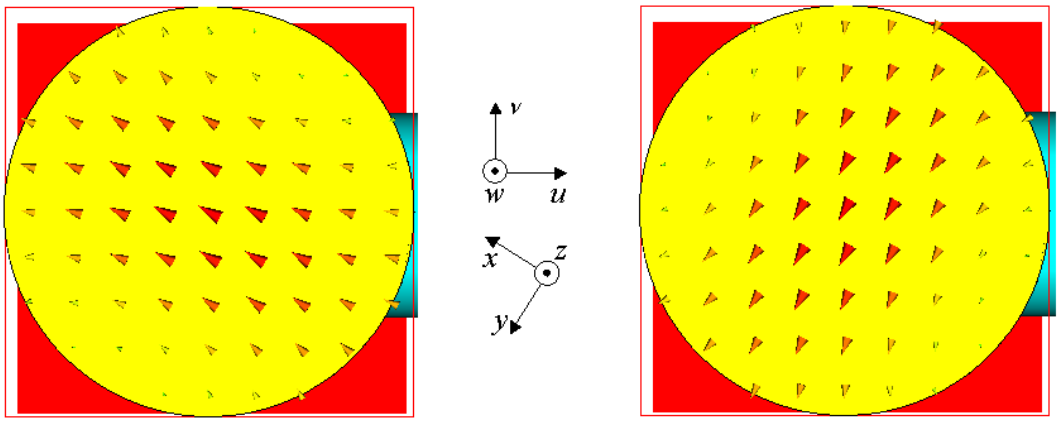

Fig. 21: Orientation of the port modes (upstream). Left picture $\mathbf{E}_{t2h,H11} = \mathbf{E}_{t3h,H11}$, H_{11} mode, horizontal polarization. Right picture $\mathbf{E}_{t2v,H11} = \mathbf{E}_{t3v,H11}$, H_{11} mode, vertical polarization.

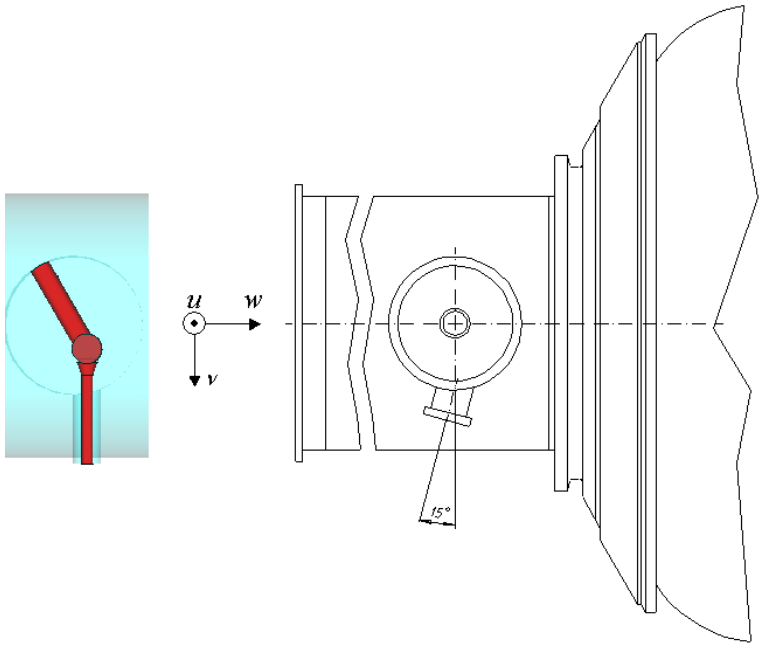

Fig. 22: Detail of DESY HOM coupler: the angle of 15° between the coaxial transmission line and the *v*-axis is neglected by the 3D model used for the discritization.

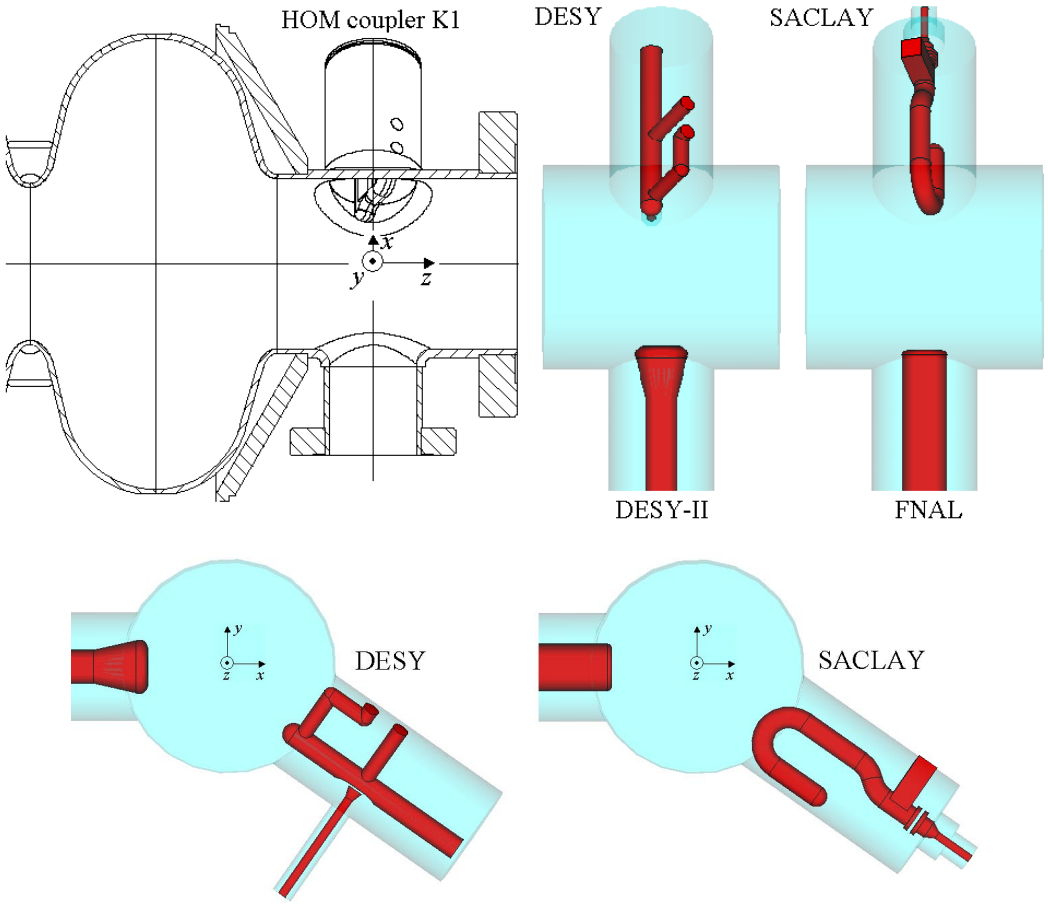

Fig. 23: Orientation of the downstream HOM coupler and of the main coupler (*x* is the horizontal coordinate, *z* is the direction of the beam). The angle between the horizontal axis and the axis of the HOM cylinder is –35°.

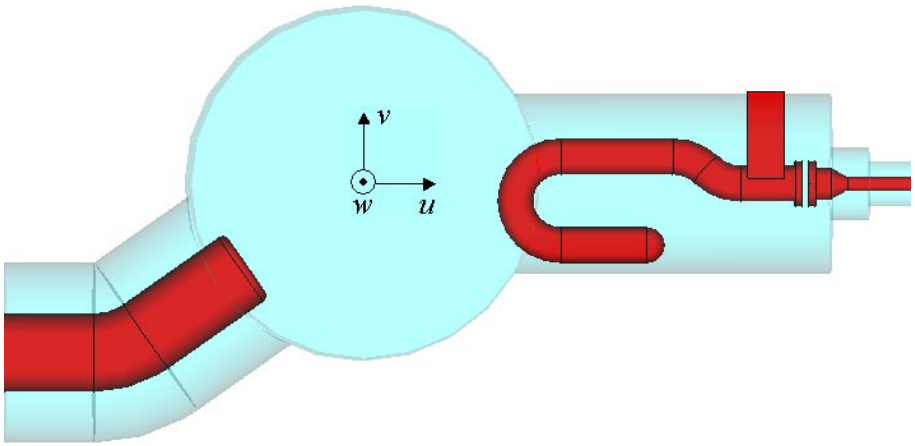

Fig. 24: Coordinate system of the rectangular *u,v,w* mesh which is used for the discretization of both coupler types (downstream).

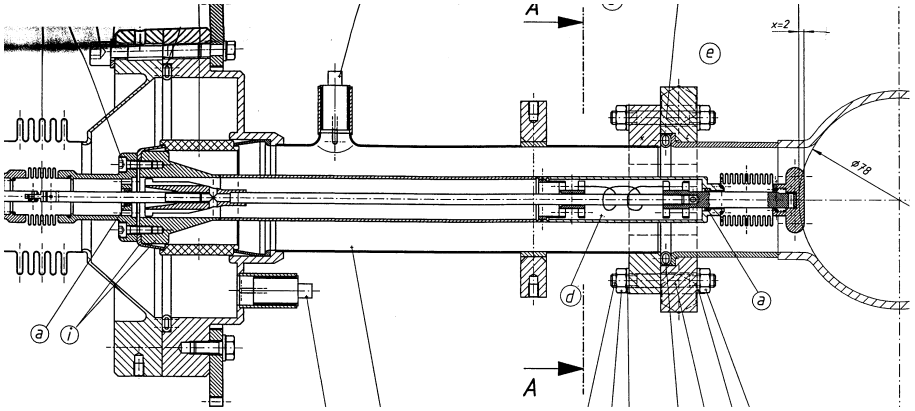

(a) DESY-I

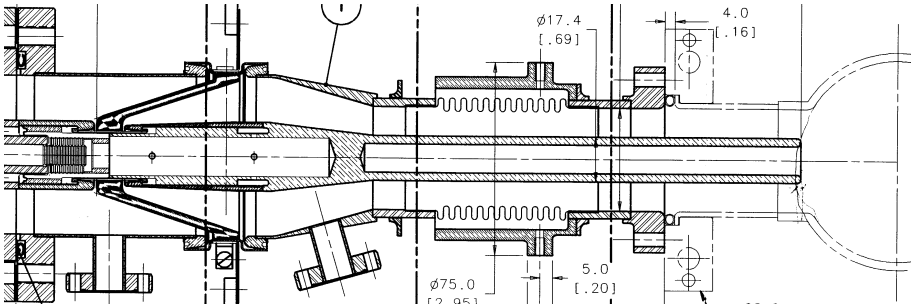

(b) FNAL

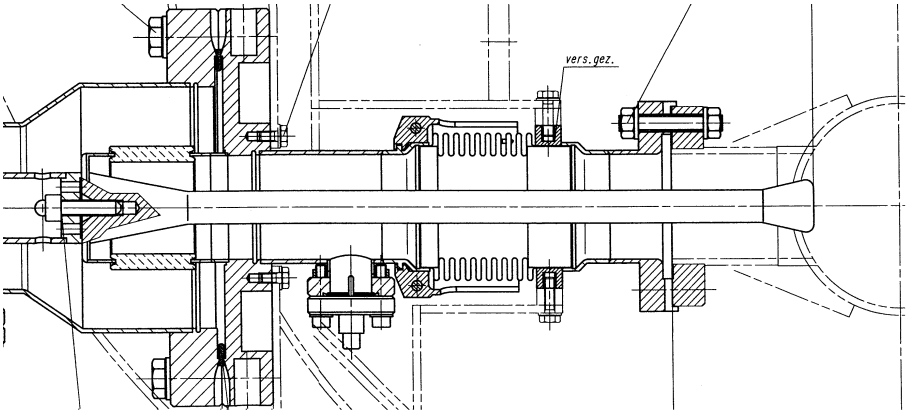

(c) DESY-II

Fig. 25: The various types of Main Coupler.

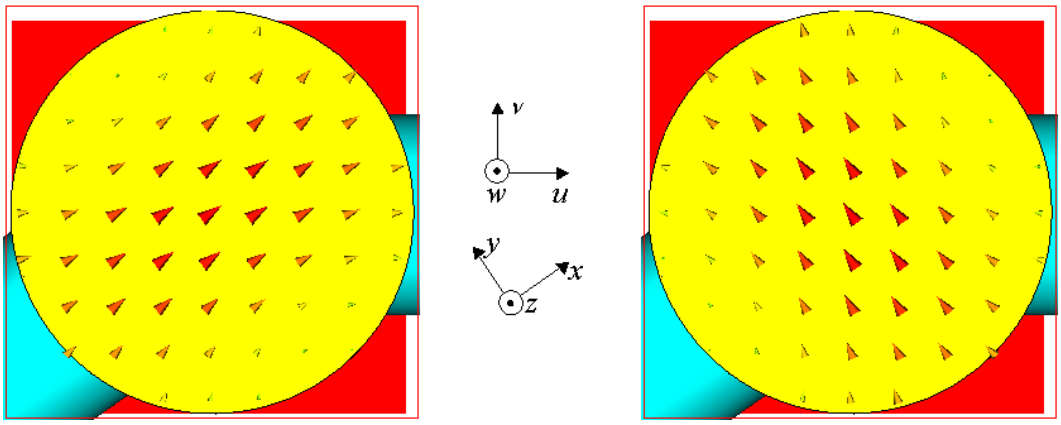

Fig. 26: Orientation of the port modes (downstream). Left picture $\mathbf{E}_{t2h,H11} = \mathbf{E}_{t3h,H11}$, H_{11} mode, horizontal polarization. Right picture $\mathbf{E}_{t2v,H11} = \mathbf{E}_{t3v,H11}$, H_{11} mode, vertical polarization.

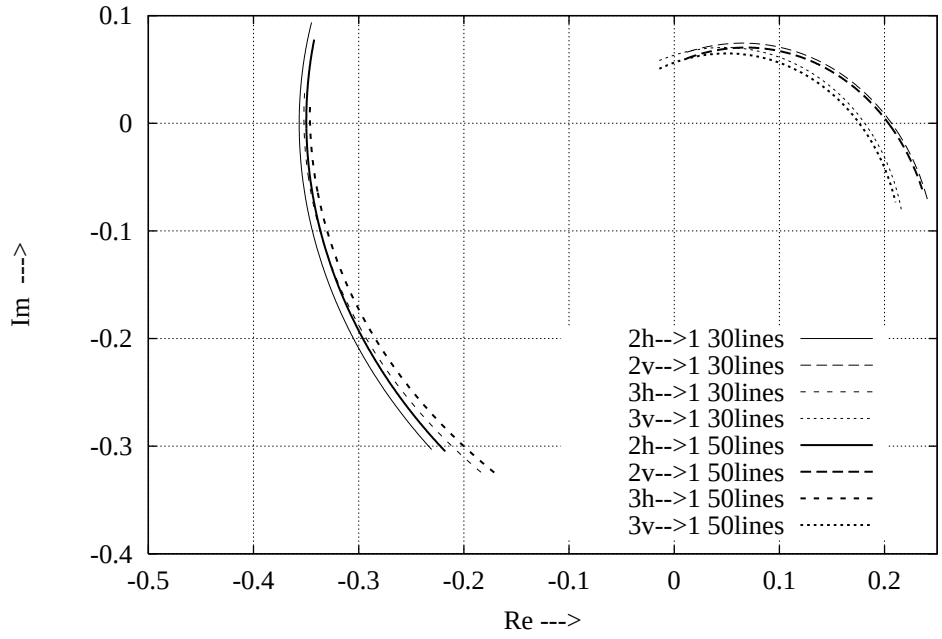

Fig. 27: Transmission coefficients $s_{1,2h}$, $4 \cdot s_{1,2v}$, $s_{1,3h}$, $4 \cdot s_{1,3v}$ from the waveguide ports to the load port of the downstream HOM/main coupler (DESY/DESY-II type) for two mesh densities (MWS parameter: 30 and 50 lines/wavelength). Port 1 is the port to the load of the HOM coupler, ports 2h and 2v are the horizontal and vertical ports on the upstream side, and ports 3h and 3v are the horizontal and vertical ports on the downstream side

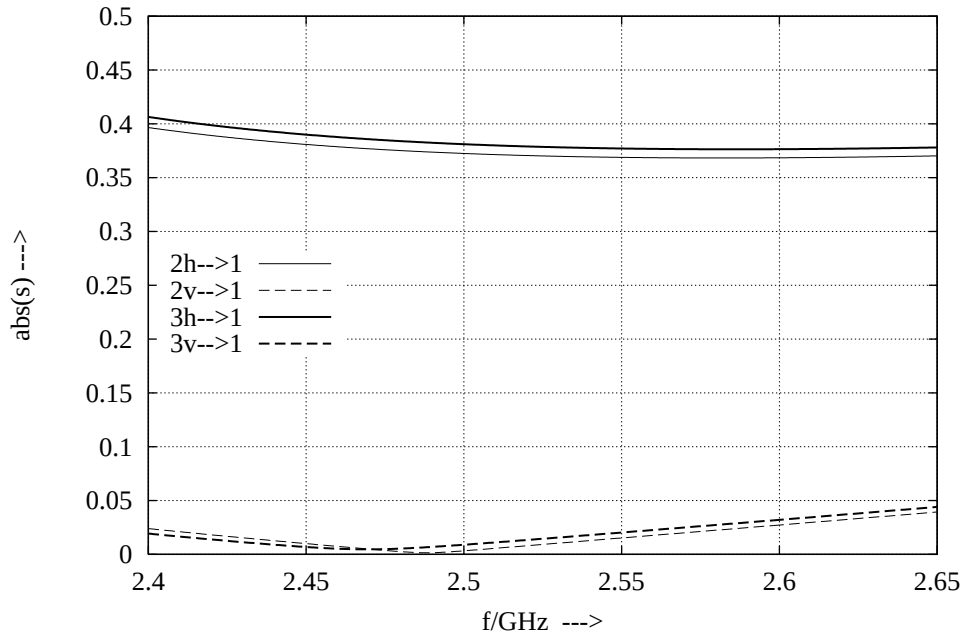

Fig. 28: Amplitude of the transmission coefficients from the waveguide ports to the load port of the upstream HOM coupler (DESY type). Port 1 is the coaxial port of the HOM coupler, ports 2h and 2v are the horizontal and vertical ports on the upstream side, and ports 3h and 3v are the horizontal and vertical ports on the downstream side.

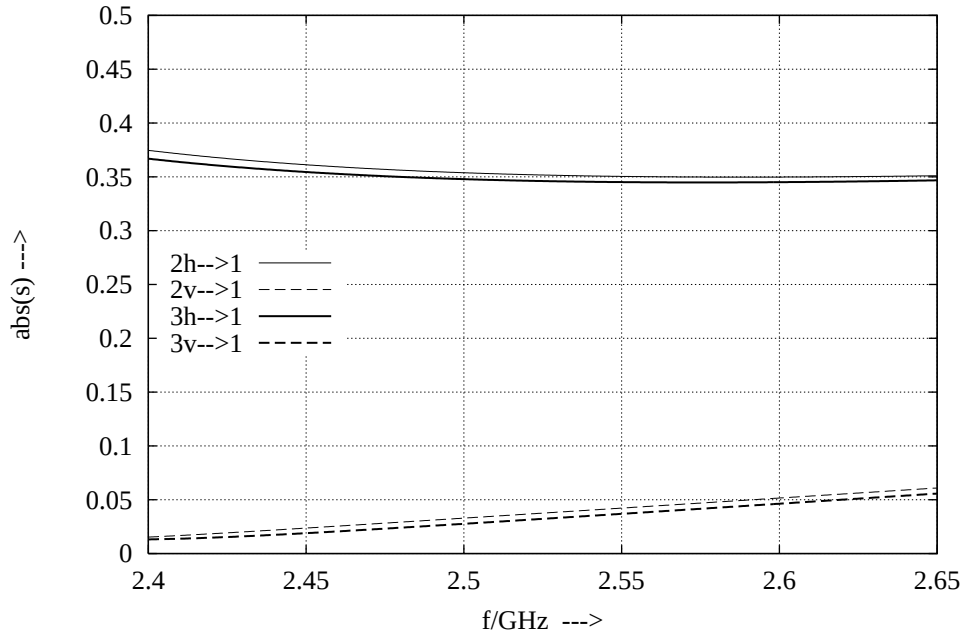

Fig. 29: Amplitude of the transmission coefficients from the waveguide ports to the load port of the downstream HOM/main coupler (DESY/DESY-II type). The port names are the same as in Fig. 28.

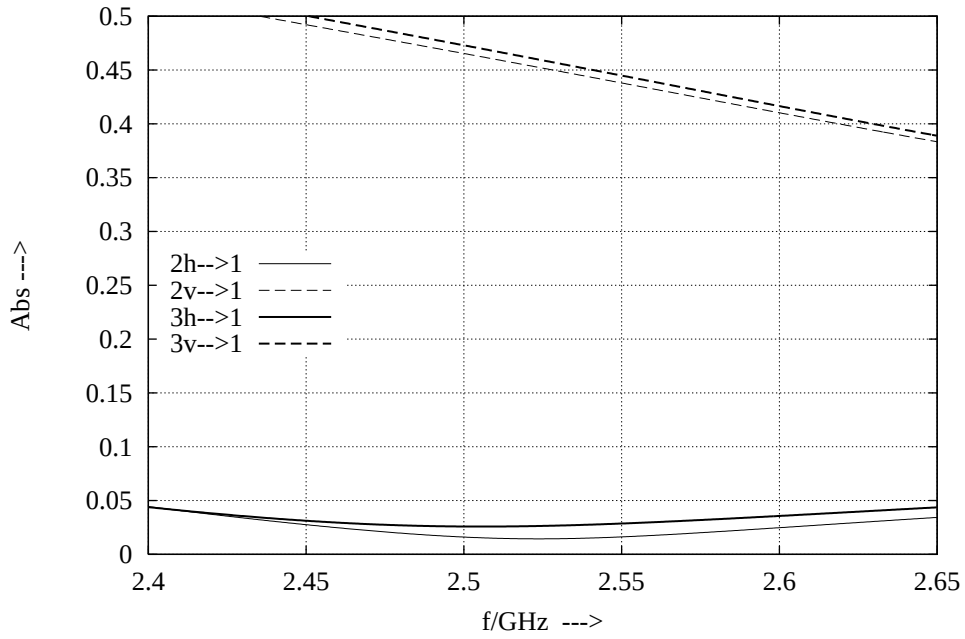

Fig. 30: Amplitude of the transmission coefficients from the waveguide ports to the load port of the upstream HOM coupler (SACLAY type). Port 1 is the port to the load of the HOM coupler, ports 2h and 2v are the horizontal and vertical ports on the upstream side, and ports 3h and 3v are the horizontal and vertical ports on the downstream side.

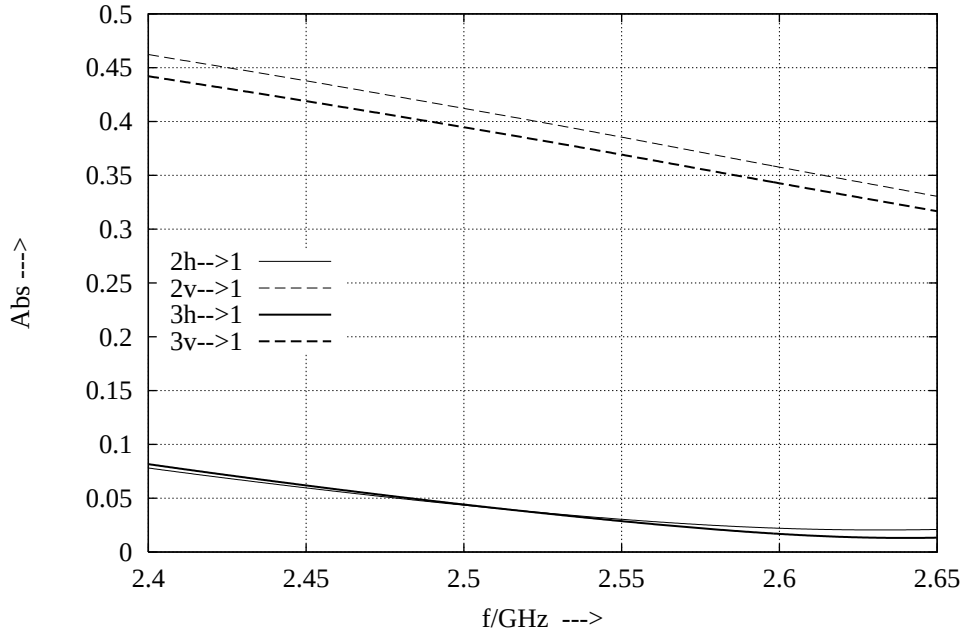

Fig. 31: Amplitude of the transmission coefficients from the waveguide ports to the load port of the downstream HOM/main coupler (SACLAY/DESY-II type). The port names are the same as in Fig. 30.

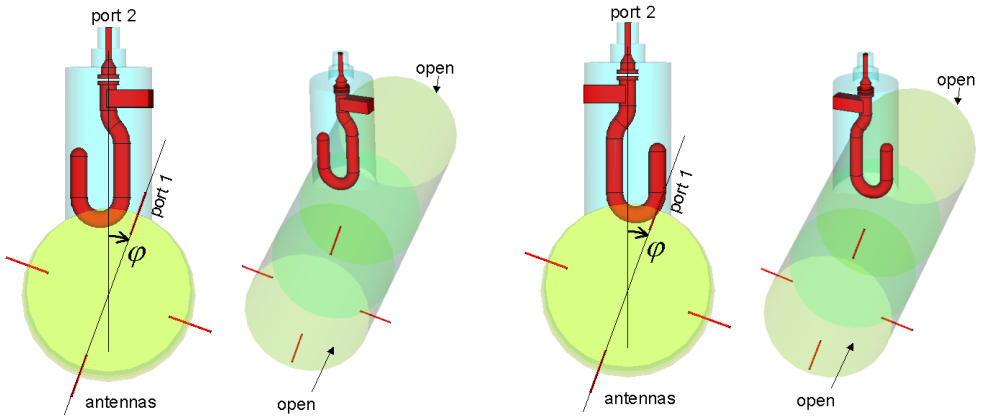

(a) (b)

Fig. 32: Measurement setup with SACLAY HOM coupler.

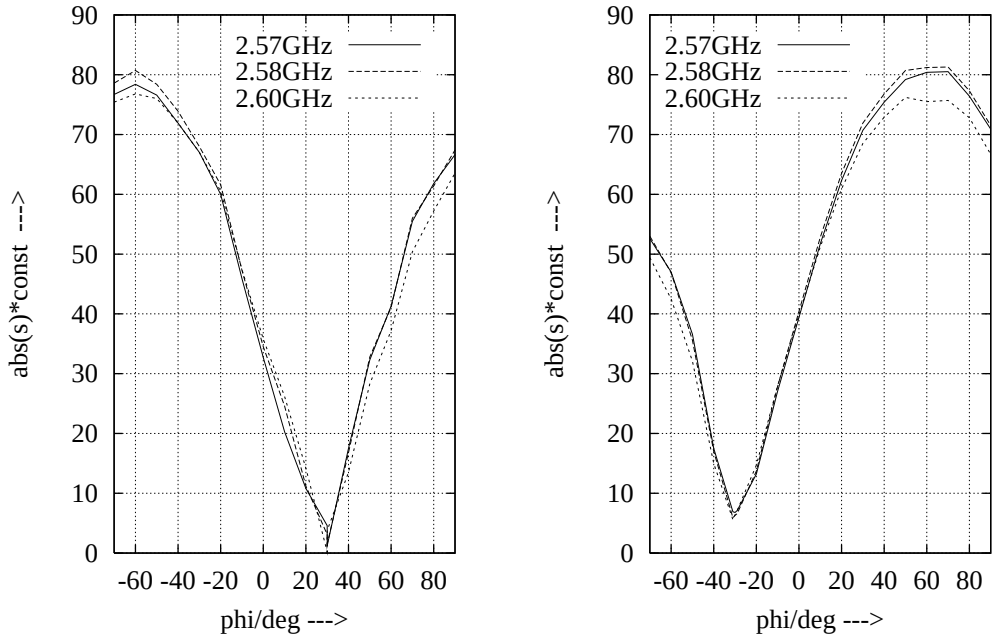

(a) (b)

Fig. 33: Measured transmission for the setup shown in Fig.32. The angle phi = 30^{o} corresponds to the horizontal plane of the SACLAY upstream coupler.

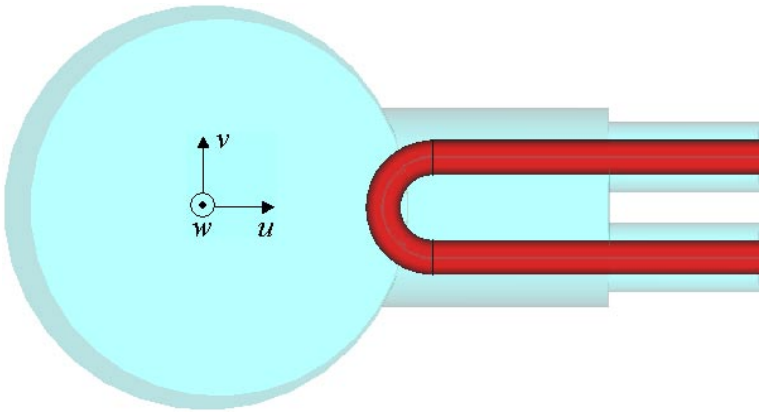

Fig. 34: Simplified geometry of a coupling loop.

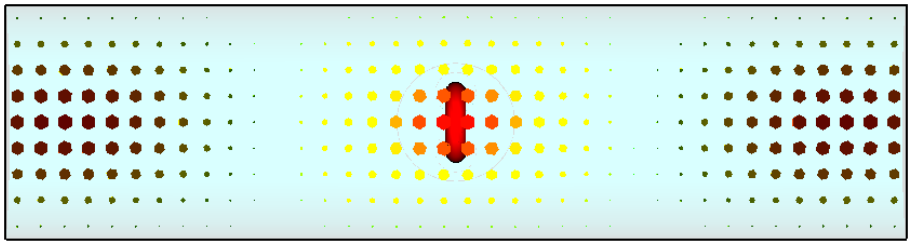

Fig. 35: A waveguide mode with u-polarization is excited by a symmetric stimulation of the coupling loop in Fig. 34.

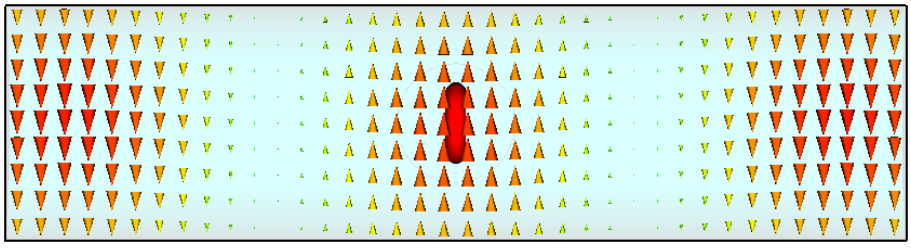

Fig. 36: An anti-symmetric stimulation of the coupling loop in Fig. 34 caused a beam-pipe mode with v-polarization.

module or multi cavity structure:

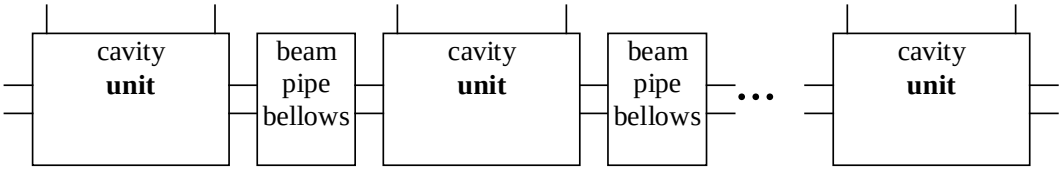

cavity unit:

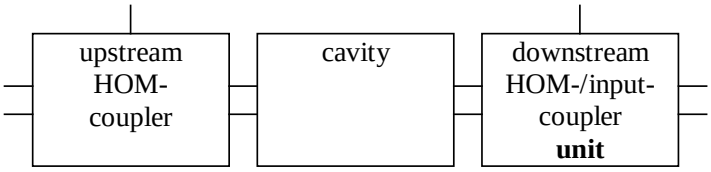

downstream HOM-/input-coupler unit:

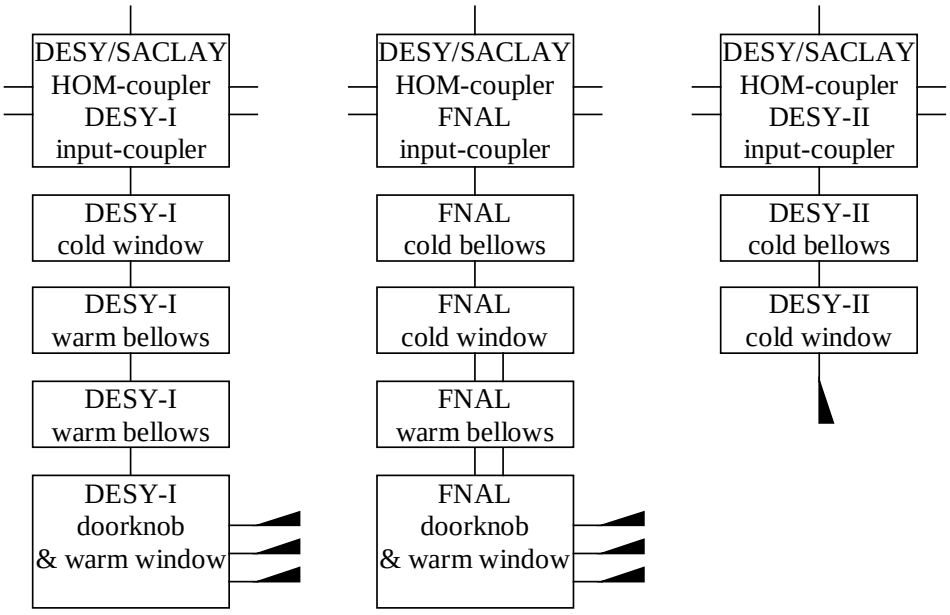

Fig. 37: Components and units of components, which are used for the calculation of scattering parameters of composed devices.

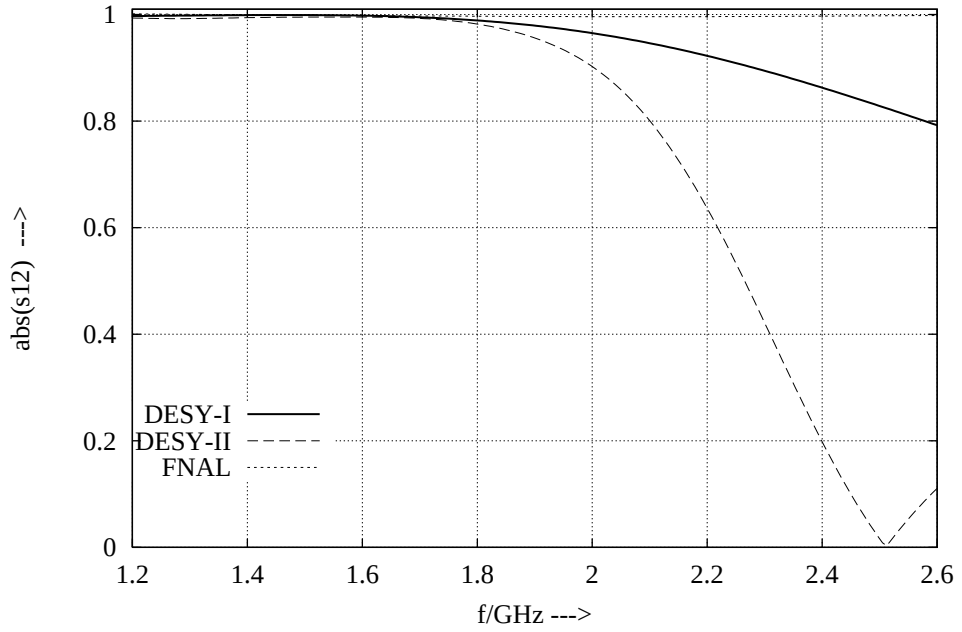

Fig. 38: Transmission through the cold windows of the DESY-I, DESY-II and FNAL main couplers.

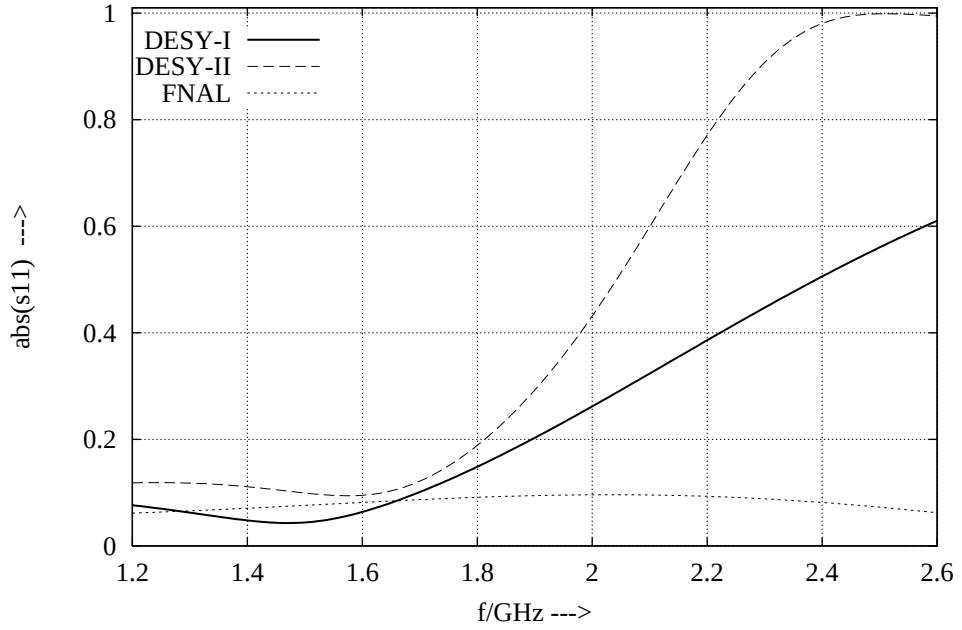

Fig. 39: Reflection coefficient of the cold windows of the DESY-I, DESY-II and FNAL main couplers.

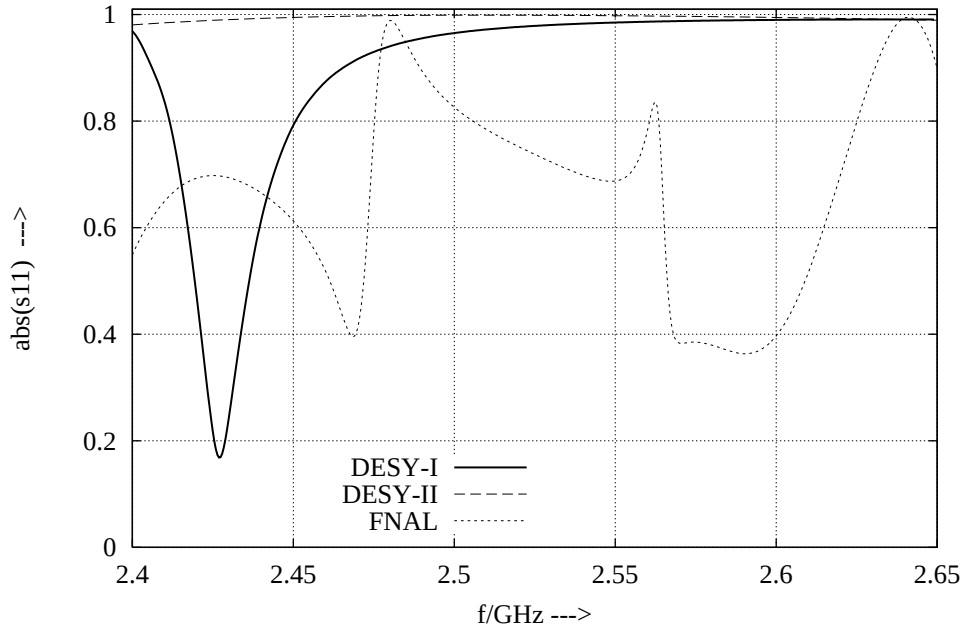

Fig. 40: Reflection coefficient of the DESY-I, DESY-II and FNAL main couplers in the reference plain between the main coupler six-port and the other components of the main coupler unit, as seen by the input coupler port. This calculation takes into account all components between the six-port and the warm waveguide (such as cold and warm windows, bellows and doorknob).

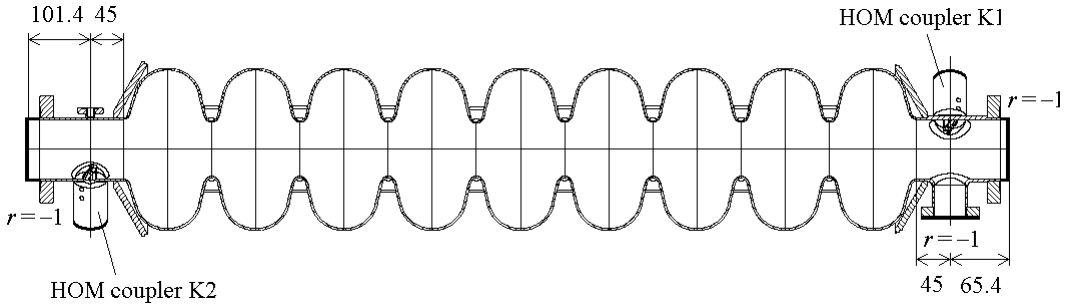

Fig. 41: Simplified setup of a test cryostat for cavity measurements. Conducting planes terminate both beam pipes and the flange for the input coupler.

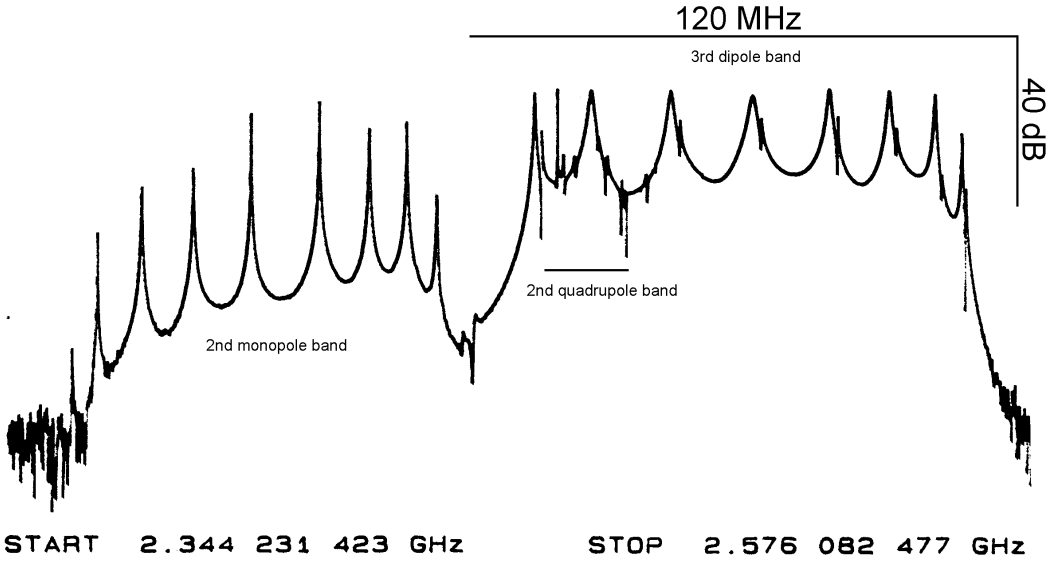

Fig. 42: Measured amplitude (in dB) of the transmission between the HOM couplers in the CHECHIA test cryostat [18].

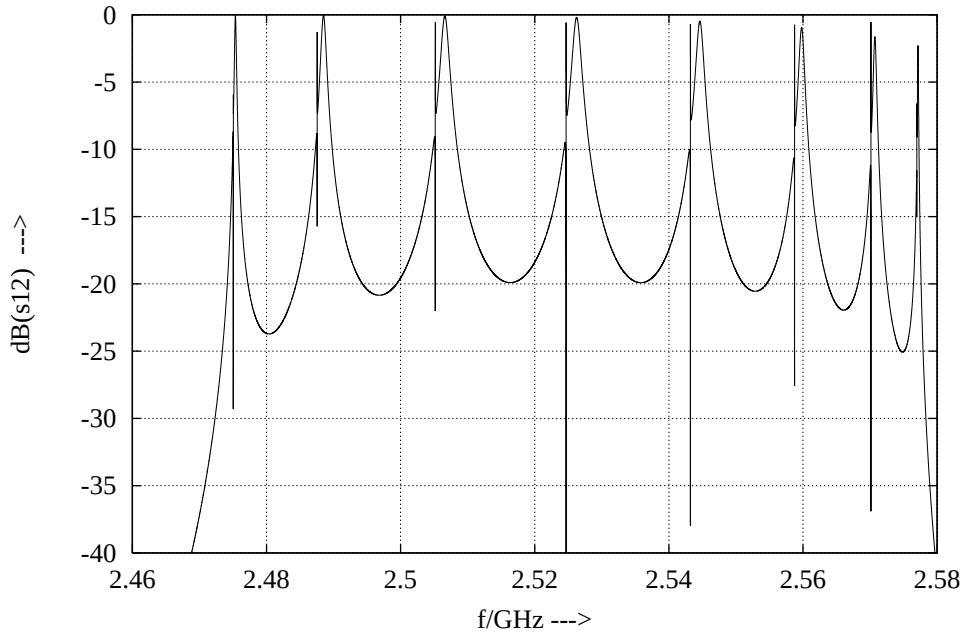

Fig. 43: DESY HOM couplers: Calculated amplitude (in dB) of the transmission between the HOM couplers in the test cryostat for the frequency range of the 3rd dipole band.

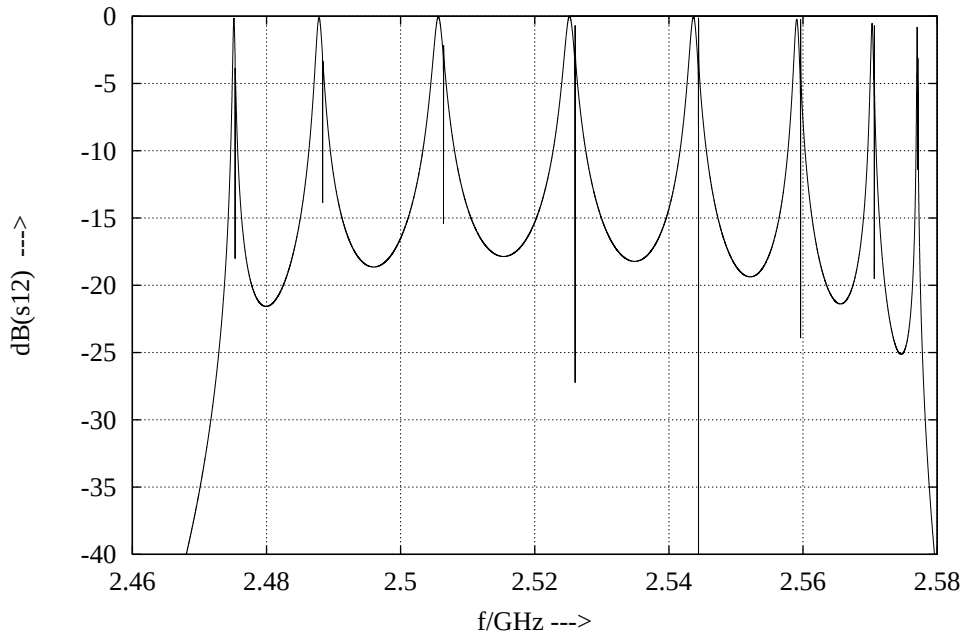

Fig. 44: SACLAY HOM couplers: Calculated amplitude (in dB) of the transmission between the HOM couplers in the test cryostat for the frequency range of the 3rd dipole band.

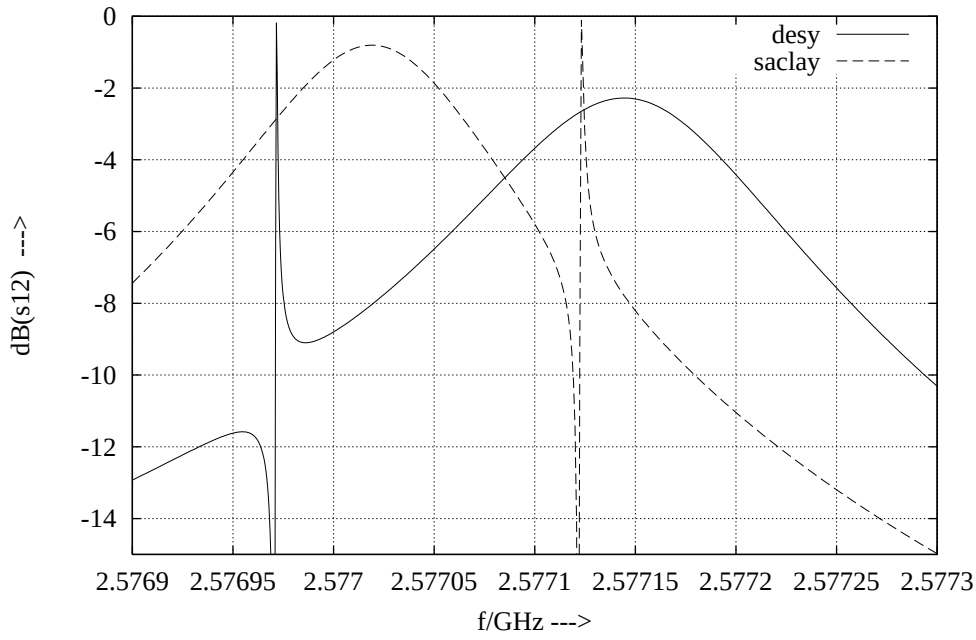

Fig. 45: Calculated amplitude (in dB) of the transmission between the HOM couplers in the test cryostat for the narrow frequency range of the last resonance of the 3rd dipole band.

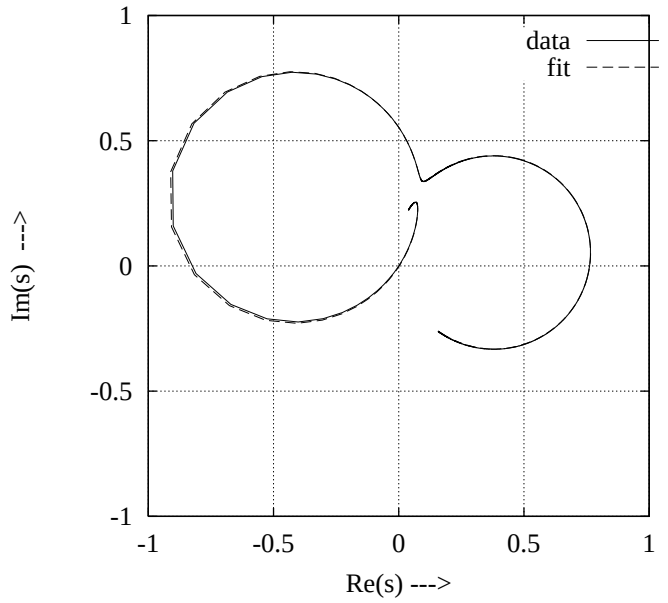

Fig. 46: DESY HOM couplers: Calculated transmission between the HOM couplers in the test cryostat for the narrow frequency range of the last resonance of the 3rd dipole band. The calculated curve (data) is fitted (fit) by a fractional rational function to determine the *Q* factor of the resonances.

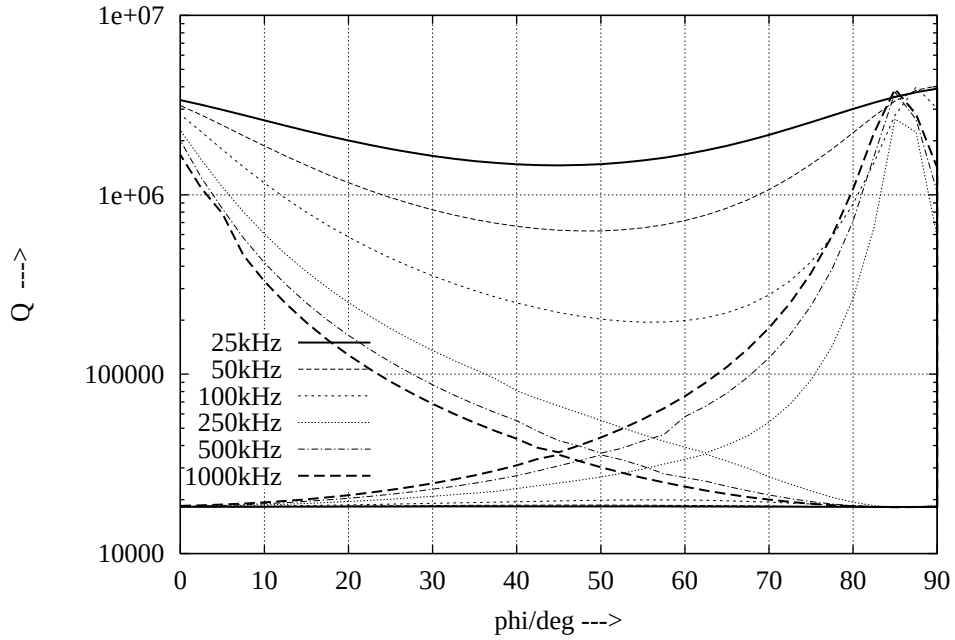

Fig. 47: Quality factors of the highest double resonance of a cavity with DESY couplers in the simplified test cryostat (cf. Fig. 41). The quality factor is plotted as function of the angle (phi) and frequency shift of the 'eigen'-polarization of the cavity.

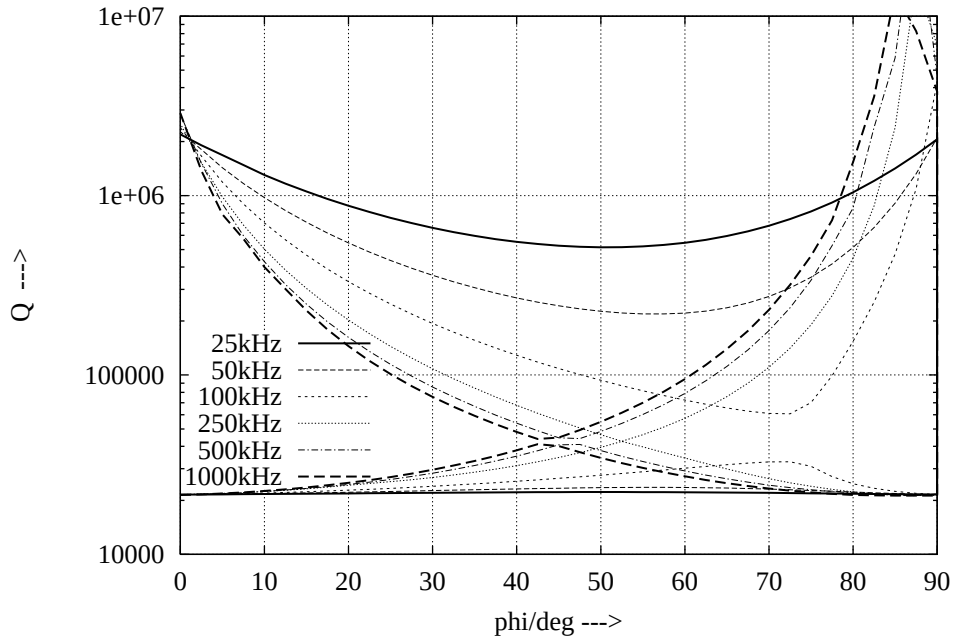

Fig. 48: Quality factors of the highest double resonance of a cavity with SACLAY couplers in the simplified test cryostat (cf. Fig. 41). The quality factor is plotted as function of the angle (phi) and frequency shift of the 'eigen'-polarization of the cavity.

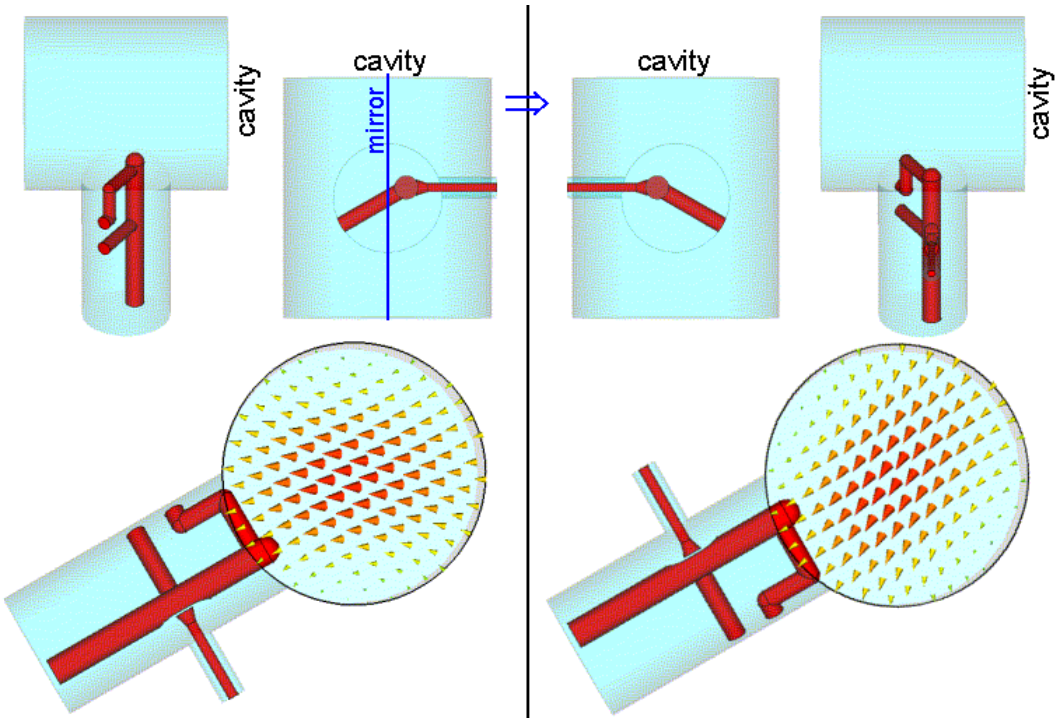

Fig. 49: Proposed modification of the upstream coupler. Due to a ‘mirror’ transformation the polarization of maximal coupling is rotated. This modification is shown for a DESY coupler, but also proposed for the SACLAY type.

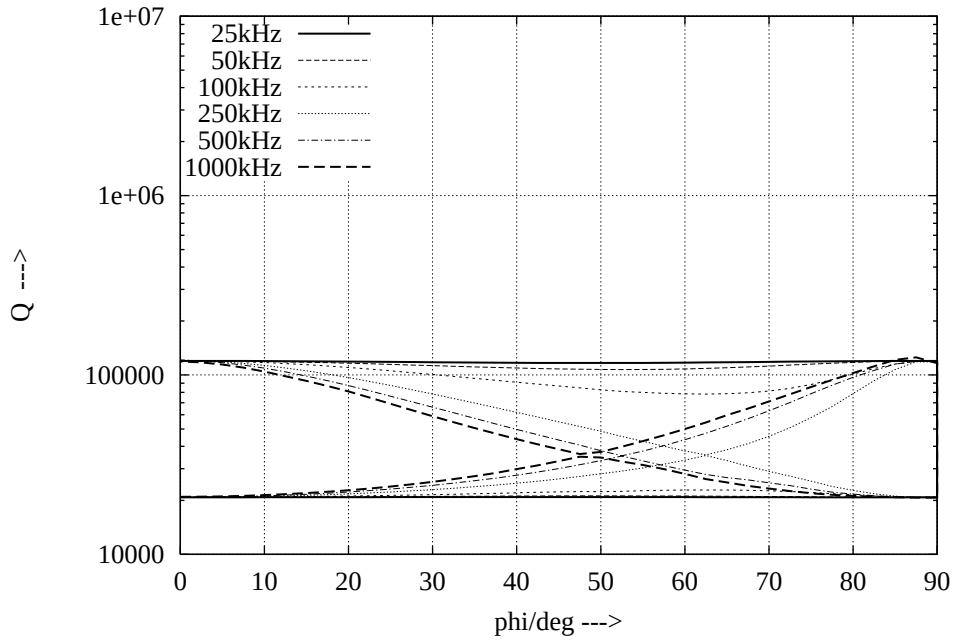

Fig. 50: Quality factors of the highest double resonance of a cavity with DESY couplers in the simplified test cryostat (cf. Fig. 41). The upstream coupler is modified as proposed in Fig.49.

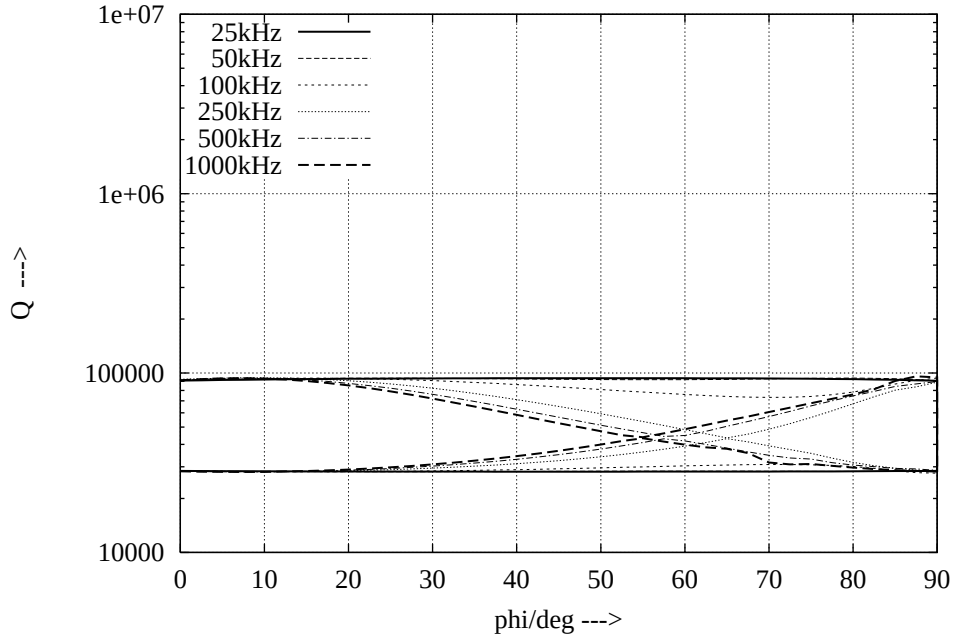

Fig. 51: Quality factors of the highest double resonance of a cavity with SACLAY couplers in the simplified test cryostat (cf. Fig. 41). The upstream coupler is modified as proposed in Fig.49.

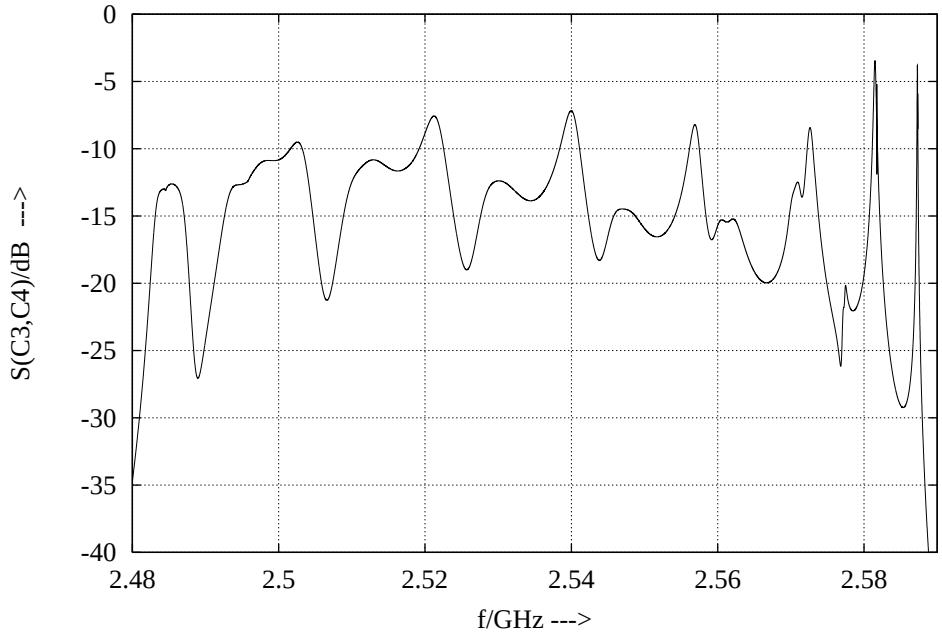

Fig. 52: Transmission between the couplers of the middle cavity of a three-cavity setup. The middle cavity is detuned by +10MHz. The coupler types are the same as for the cavities S8,D10,D1 in module 1.

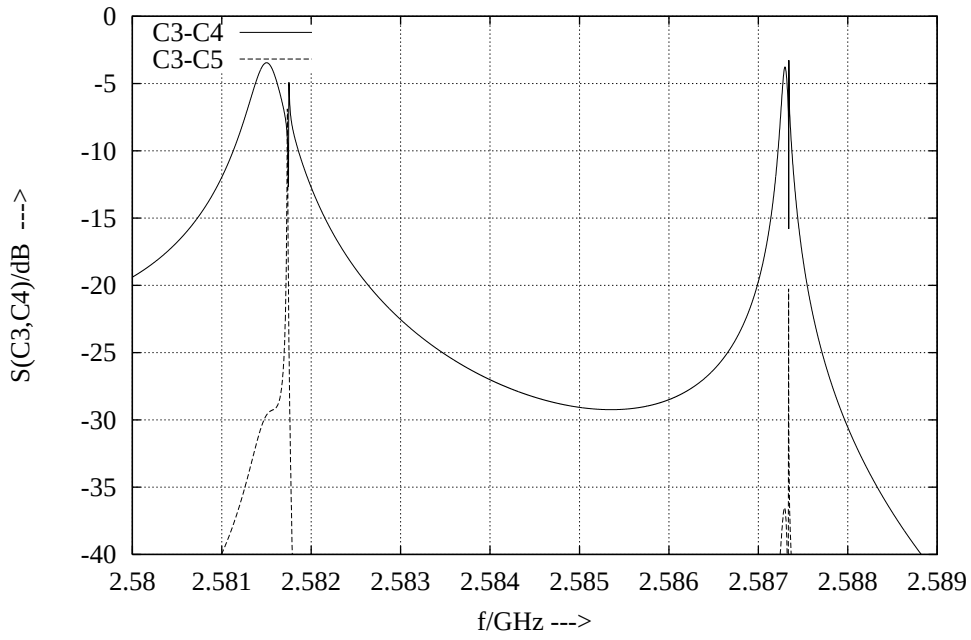

Fig. 53: Transmission in a narrow frequency range for the same setup as in Fig. 52. Solid line: transmission between the couplers of the middle cavity, dashed line: transmission between the upstream couplers of cavity 2 and cavity 3.

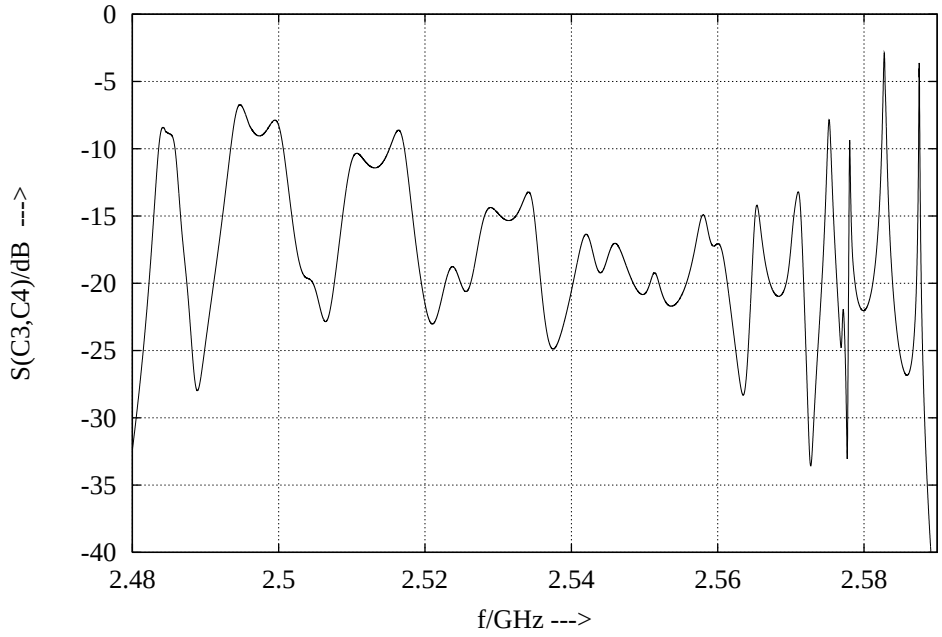

Fig. 54: Transmission between the couplers of the middle cavity of a three-cavity setup. The middle cavity is detuned by +10MHz. The coupler types are the same as for the cavities D2,S11,D4 in module 1.

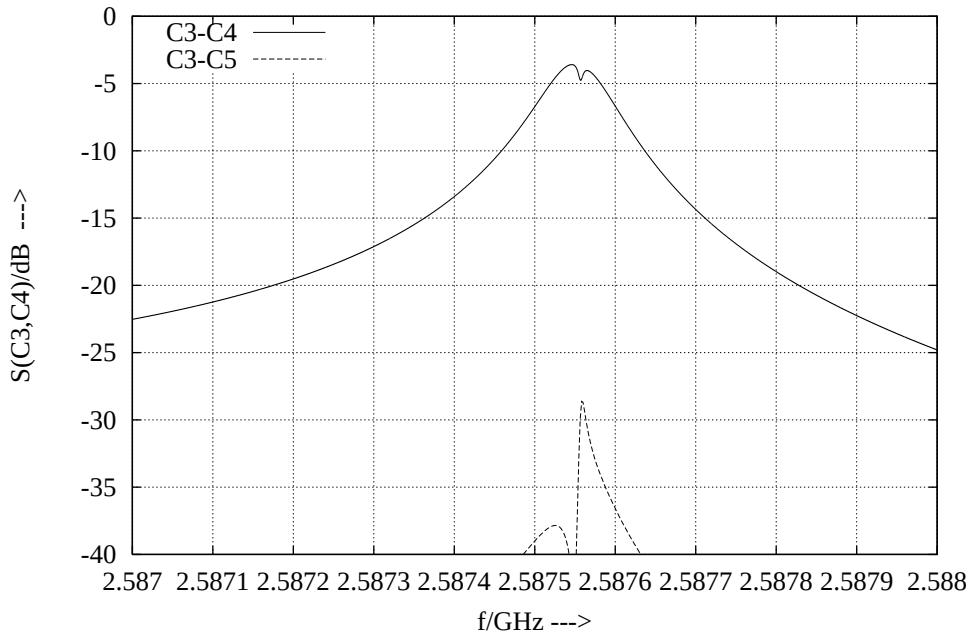

Fig. 55: Transmission in a narrow frequency range for the same setup as in Fig. 54. Solid line: transmission between the couplers of the middle cavity, dashed line: transmission between the upstream couplers of cavity 2 and 3.

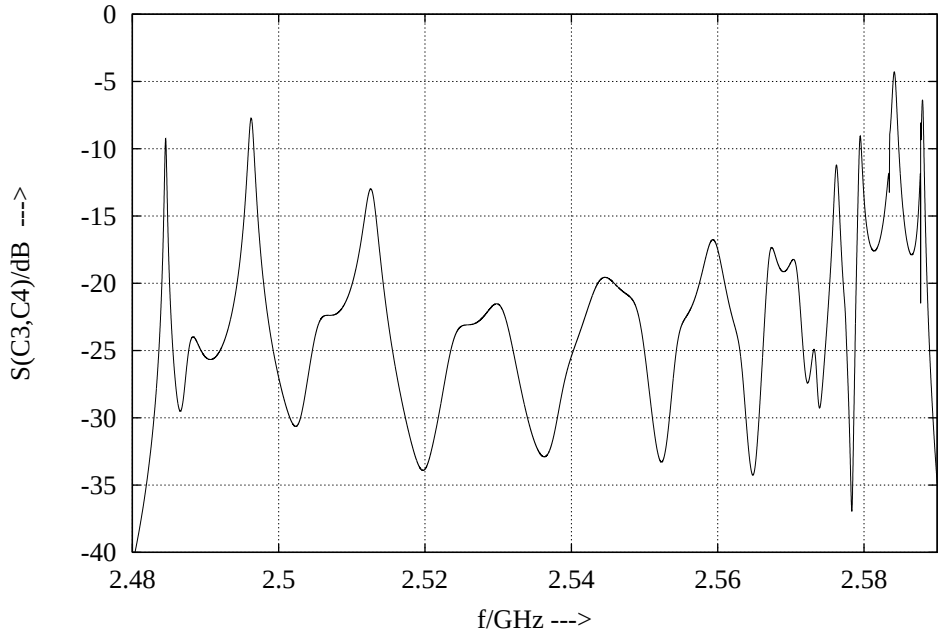

Fig. 56: Transmission between the couplers of the middle cavity of a three-cavity setup. The middle cavity is detuned by +10MHz. The coupler types are the same as for the cavities C23,A15,C26 in module 2.

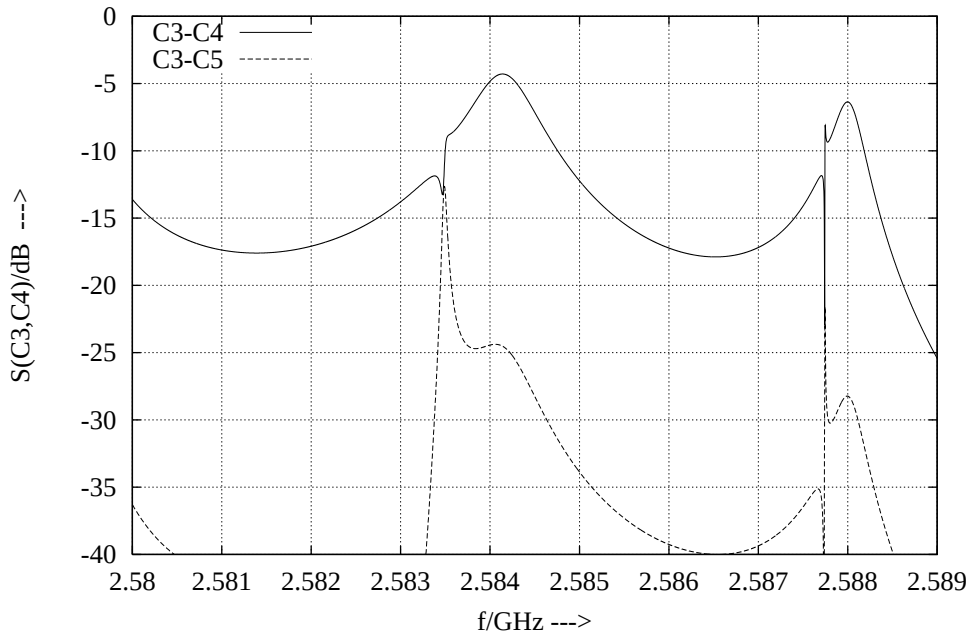

Fig. 57: Transmission in a narrow frequency range for the same setup as in Fig. 56. Solid line: transmission between the couplers of the middle cavity, dashed line: transmission between the upstream couplers of cavity 2 and 3.

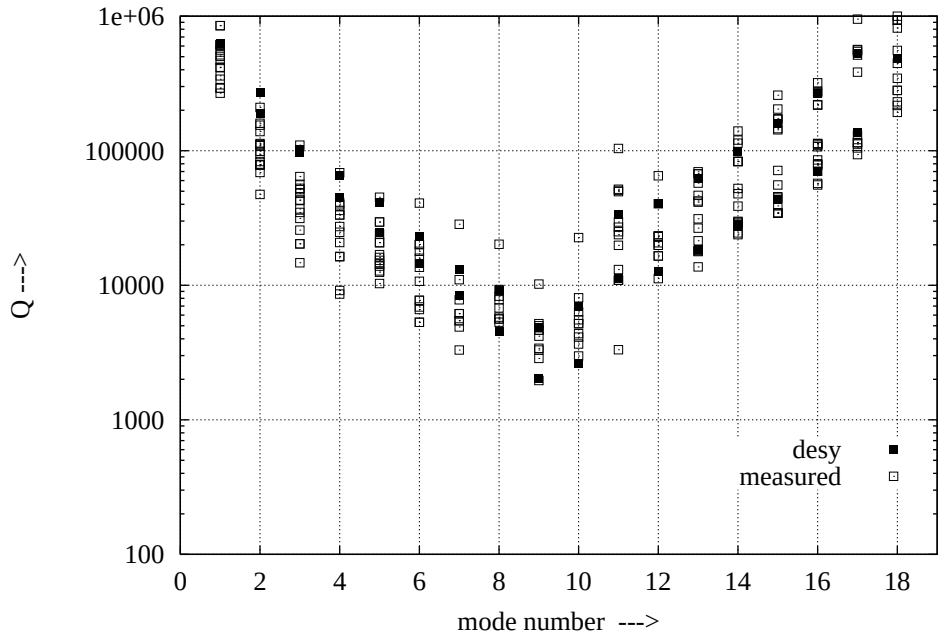

Fig. 58: Calculated and measured quality factors of the modes in the 1st and 2nd dipole band for a cavity with DESY HOM couplers: 'desy' calculated values, 'measured' measured values for eight different cavities [18].

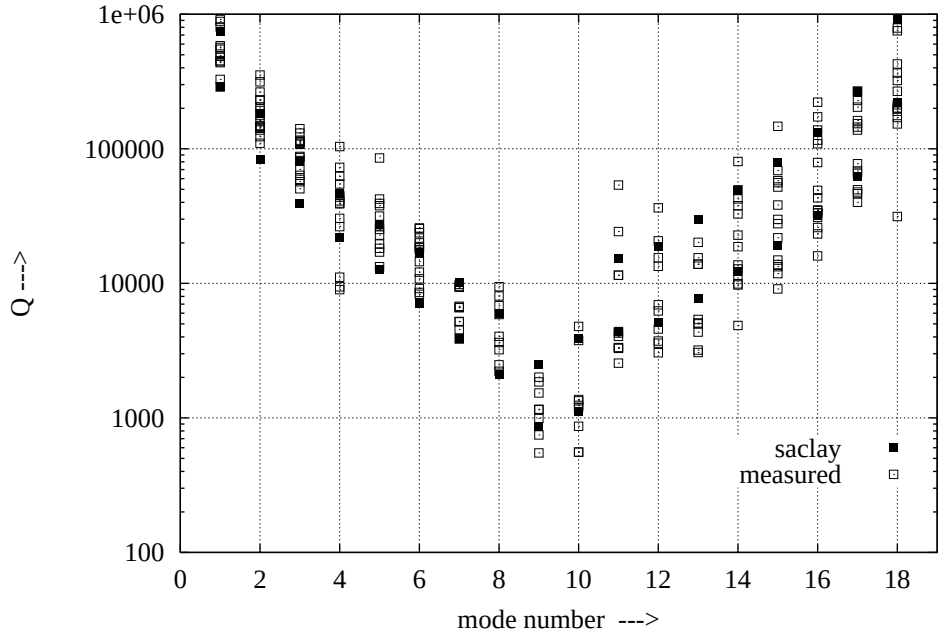

Fig. 59: Calculated and measured quality factors of the modes in the 1st and 2nd dipole band for a cavity with SACLAY HOM couplers: 'saclay' calculated values, 'measured' measured values for eight different cavities [18].

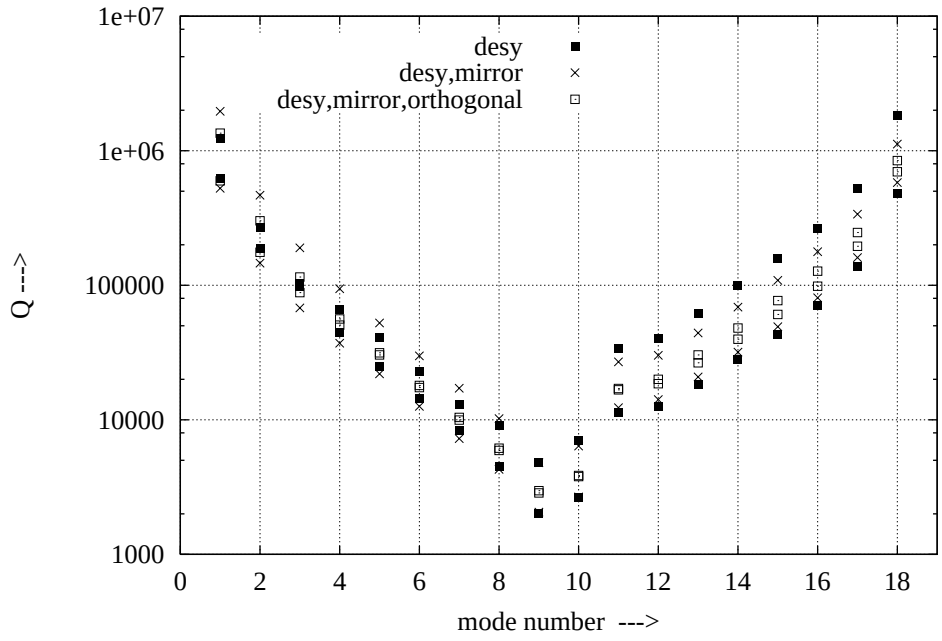

Fig. 60: Calculated quality factors of the modes in the 1st and 2nd dipole band: 'desy' cavity with DESY HOM couplers, 'desy,mirror' modified upstream coupler , 'desy,mirror,orthogonal' modified upstream coupler orthogonal to the downstream HOM coupler.

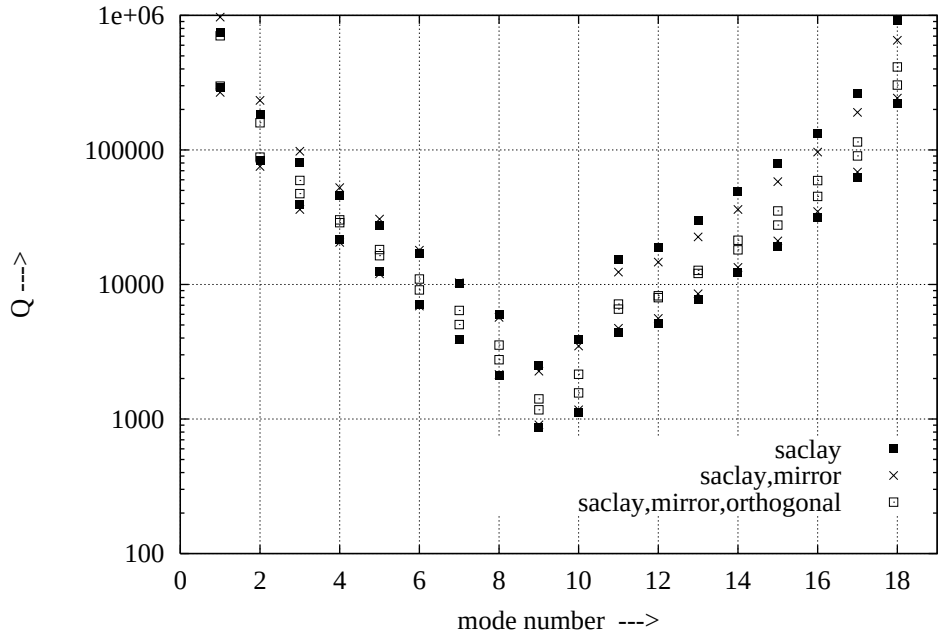

Fig. 61: Calculated quality factors of the modes in the 1st and 2nd dipole band: 'saclay' cavity with SACLAY HOM couplers, 'saclay,mirror' modified upstream coupler , 'saclay,mirror,orthogonal' modified upstream coupler orthogonal to the downstream HOM coupler.